After-hyperpolarization Currents and Acetylcholine Control

Sigmoid Transfer Functions in a Spiking Cortical Model

Jesse Palma, Massimiliano Versace, and Stephen Grossberg

Center for Adaptive Systems,

Department of Cognitive and Neural Systems,

and Center of Excellence for Learning in Education, Science, and Technology,

Boston University

677 Beacon Street, Boston, MA 02215, USA

Corresponding Author:

Stephen Grossberg

Email: steve@bu.edu

Telephone: 617-353-7858/7

Fax: 617-353-7755

Abstract

Recurrent networks are ubiquitous in the brain, where they enable a diverse set of transformations during perception, cognition, emotion, and action. It has been known since the 1970's how the choice of feedback signal function can control the transformation of input patterns to rate-based recurrent on-center off-surround networks into activity patterns that are stored in short term memory. A sigmoid signal function may, in particular, control a quenching threshold below which inputs are suppressed as noise and above which they may be contrast enhanced before the resulting activity pattern is stored. The threshold and slope of the sigmoid signal function determine the degree of noise suppression and of contrast enhancement. This article analyses how sigmoid signal functions and their shape may be determined in biophysically realistic spiking neurons. Combinations of fast, medium, and slow after-hyperpolarization (AHP) currents, and their modulation by acetylcholine (ACh), can control sigmoid signal threshold and slope. Instead of a simple gain in excitability that was previously attributed to ACh, cholinergic modulation may cause translation of the sigmoid threshold. This property clarifies how activation of ACh by basal forebrain circuits, notably the nucleus basalis of Meynert, may alter the *vigilance* of category learning circuits, and thus their sensitivity to predictive mismatches, thereby controlling whether learned categories code concrete or abstract information, as predicted by Adaptive Resonance Theory.

1 Introduction

1.1 Pattern transformation and short-term memory storage by recurrent competitive networks

Networks of neurons can perform complex nonlinear transformations of activity patterns. Rate-based recurrent neural networks enable a diverse set of nonlinear transformations useful for cognitive functions, including short-term memory storage (Grossberg 1973), syntactic structure in linguistic processing (Elman 1991), motor coordination and execution (Bullock, Cisek, and Grossberg, 1998; Bullock and Grossberg 1988), and incremental learning of recognition categories (Carpenter and Grossberg 1987, 1991). Anatomical studies have confirmed that recurrence is a prevalent feature in brain systems (e.g., Bosking et al. 1997; Chisum et al. 2003; Levitt et al. 1994; Morishima and Kawaguchi 2006; Schmidt et al. 1997; Song et al. 2005).

Within recurrent networks, the form of signaling at the cellular scale has a major impact on network transformations of input patterns. Beginning in Grossberg (1973), theorems proved about rate-based neural models have provided insights into how the choice of the feedback signal functions in recurrent networks can alter how input patterns are transformed (e.g., Ellias and Grossberg 1975; Grossberg and Levine 1975; Wersing et al. 2001). Early theorems (e.g., Grossberg, 1973) analyzed how signal functions in recurrent on-center off-surround networks whose cells obey membrane, or shunting, equations (see Fig. 1a and Eqs. (11)-(14)) transform input patterns before they are stored in short term memory as sustained patterns of neural activity as the network settles to equilibrium. In these simplest networks, the on-center of self-excitatory feedback is narrow, and the off-surround of lateral inhibition reaches all other cells.

As shown in Fig. 1b, if the signal function is linear (e.g., $f(x) = Ax$), then the relative activities of the initial input pattern are preserved. If the signal function is slower-than-linear (e.g., $f(x) = Ax(B-x)^{-1}$), then all differences in the input are uniformized. In both of these cases, noise is amplified. If a signal function is faster-than-linear (e.g., $f(x) = Ax^2$), then noise is suppressed. In fact, noise is suppressed so vigorously, than only the cell (population) with the largest input survives the competition, and its activity is stored in short term memory. This is thus a winner-take-all (WTA) network.

In order to enable cells with activities less than the maximum to be stored in short term memory, a sigmoid, or S-shaped, signal function suffices, because it is a hybrid of the other signal functions. Any signal function needs to be faster-than-linear at low activity levels in order to suppress noise. And any biologically plausible signal function needs to be bounded at high activity values. A sigmoid signal function is the simplest one that combines both constraints. At high activity values, it is slower-than-linear. Because it is faster-than-linear at low activities, it is approximately linear at intermediate activities, by continuity. Thus, a sigmoid signal function can begin to contrast-enhance an input pattern as the shunting on-center off-surround network interactions begin to normalize cell activities and drive them into the approximately linear range, where they can be stored as a partially contrast-enhanced pattern; namely, an activity pattern in which a subset of the most active cells are contrast-enhanced and stored in short-term memory, while activities of less active cells are completely suppressed.

The net effect on network dynamics is to define a *quenching threshold*, or initial activity level below which activities are treated like noise and suppressed, and above which they are contrast-enhanced and stored in short term memory. The quenching threshold can be tuned, thus leading to a tunable filter: In the limit of a high quenching threshold, it can perform like a WTA network. If in response to an unexpected event the quenching threshold goes down, then the

network can store a distributed pattern of input features, until hypothesis testing can select the features that can better predict future outcomes. See Section 4.2.
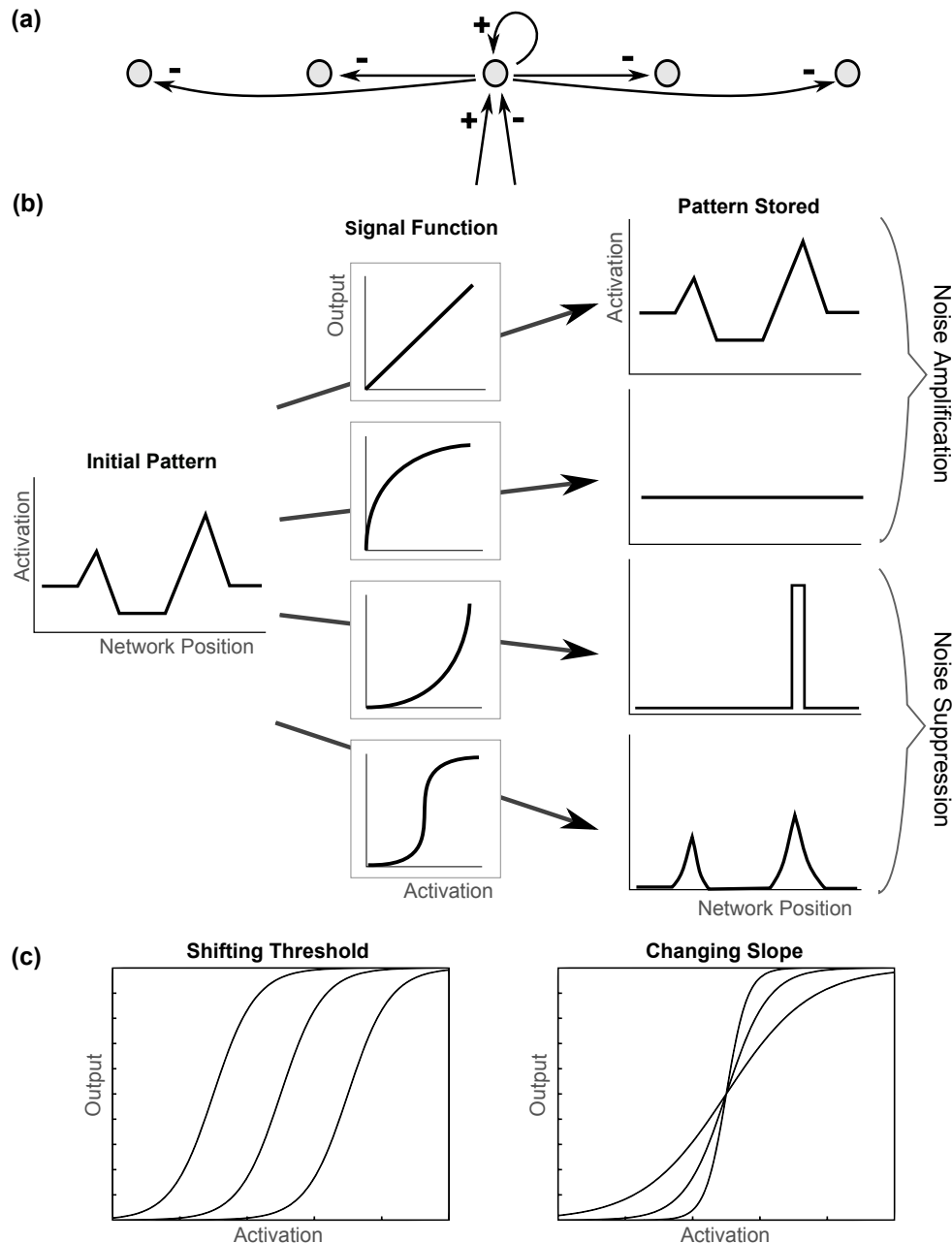
Fig. 1 Dynamics of signal functions in a recurrent architecture. (**a**) Recurrent architecture with self-excitation and lateral inhibition in a classical neural network. (**b**) How the choice of four different nonlinear signal function determines network storage behavior including whether noise is amplified or suppressed (Grossberg 1973). The sigmoidal case is noteworthy, because it features a quenching threshold. (**c**) Threshold translation and slope change of a sigmoid signal function can alter how the signal function transforms initial input patterns before they are stored in short-term memory

What processes control the shape of sigmoid signal functions within biophysically detailed models of spiking neurons? In networks of spiking neurons, transfer functions, defined as the relationship between input and output spiking rates, are postulated to act analogously to the signal functions that are used in rate-based models. Physiological observations confirm that neurons often exhibit a sigmoidal relationship between input and output (Fellous et al. 2003; Freeman 1979). For a sigmoidal curve, apart from rescaling by boosting excitability, there are two elementary degrees of freedom: threshold translation and slope change (Fig. 1c). Translation of the sigmoidal threshold occurs when the region of highest sensitivity for the function shifts along the input domain, and mathematically equates to movement of its point of inflection. Slope varies when the curve either steepens or becomes more gradual, and mathematically relates to the magnitude of the derivative around the point of inflection. Because biological cell activation is limited to a restricted operational domain, threshold translation and slope alterations could manipulate the effective curvature of the signaling function. What factors adaptively shape the two sigmoidal degrees of freedom during development or even regulate them dynamically to modulate behavior in real time?

1.2 After-hyperpolarization currents alter sigmoid signals
After-hyperpolarization (AHP) currents, defined as hyperpolarizing currents that occur following action potentials, present prime candidates for adaptive control of cell transfer functions, because of their dependence on recent activity and their susceptibility to external modulation. These AHP currents are predominantly carried by calcium-dependent potassium channels (Hotson and Prince 1980; Lancaster and Adams 1986), but also partly by calcium-independent potassium currents (Lorenzon and Foehring 1992). Calcium (Ca^{2+}) dependence implies spike dependence, because calcium concentrations fluctuate via voltage-dependent channels that open as a result of depolarizations during action potentials. *In vitro* studies of these currents in large layer 5 Betz cells of cat sensorimotor cortex (Schwindt et al. 1988b) have identified three distinct AHP currents: a fast, medium, and slow current. Henceforth, we refer to these currents as fAHP, mAHP and sAHP, respectively. A study of pyramidal cells in layers 3-6 of human neocortex (Lorenzon and Foehring 1992) revealed three currents with similar temporal profiles and pharmacological properties to the earlier study, and recent reports confirm similar mAHP and sAHP currents in a variety of rat tissue preparations (Lee et al. 2005; Storm 1987). In certain recordings, the sAHP appears to further divide into an early and late sAHP (Schwindt et al. 1988b), although this result is not consistent across studies. The difference in the time course of these AHP currents has not been completely explained, but recent evidence suggests that proximity to calcium channels may be the dominant factor rather than, for example, the time constant of calcium binding to the channels themselves (Lima and Marrion 2007).

This paper demonstrates how the collective state of the three AHP conductances can control the shape of sigmoidal transfer functions by independently translating its threshold and changing its slope. The analysis reveals simple rules that govern conductance changes in the three AHP currents as they combine to generate desired changes in signaling. In so doing, we identify conservation laws for maintaining the asymptote of the transfer function, or upper bound on neuronal firing. We establish that the sigmoid threshold shifts lower when sAHP and mAHP decrease while fAHP increases, at the appropriate ratios. We demonstrate that the slope becomes steeper when sAHP and fAHP decrease while mAHP increases, at the appropriate ratios.

1.3 Acetylcholine alters after-hyperpolarization current

Numerous studies have shown that AHP currents are modulated by the level of acetylcholine (ACh) and other neurotransmitters (McCormick and Williamson 1989; Vogalis et al. 2003 for review). ACh is believed to increase gain on sensory input in cortical cells both by reducing AHP currents as well as strengthening sodium currents to boost cell excitability (Giocomo and Hasselmo 2007; Sarter et al. 2005). This description and associated computational models portray ACh as a promoter of sensory processing by decrease in a single AHP current either by lumping distinct AHP currents together or neglecting two of the three currents.

How does ACh biophysically coordinate the control of AHP currents at all three different timescales? The current model proposes that ACh modulates the three AHP currents, and thus sigmoid signal shape, by shifting the threshold in the manner described in Fig. 1(c). Changes in the AHP currents can cause a steepening in the sigmoid slope or cause a shift in the sigmoid threshold.

Previous neural models have addressed the effect of ACh on AHP currents (Barkai and Hasselmo 1994; Cox et al. 1997; Grossberg and Versace 2008; Soto et al. 2006; Wang et al. 2003). However, they have not accounted for the full breadth of timescales on which AHP currents have been observed. For example, a model of pyramidal cells from piriform cortex treated ACh modulation as a decrease in a slow AHP current and a voltage-dependent potassium current, called m-current, because of its sensitivity to the ACh agonist, muscarine, a contributor to the mAHP current (Barkai and Hasselmo 1994).

In Adaptive Resonance Theory, or ART, augmented cortical excitability due to predictive mismatch may cause reset of currently active cognitive recognition codes, or categories, even in cases where top-down feedback may earlier have partially matched bottom-up input. This increase of excitability is mediated by the gain, called *vigilance*, of the process whereby bottom-up input patterns are matched against learned top-down expectations (Carpenter and Grossberg, 1987, 1991). Grossberg and Versace (2008) proposed that the release of ACh might increase vigilance and thereby promote search for and learning of more specific, or concrete, recognition categories in response to mismatch-inducing environmental feedback. In particular, Grossberg and Versace (2008) proposed that mismatch-mediated activation of the nucleus basalis of Meynert results in release of ACh, which causes a reduction of an AHP current in layer 5 pyramidal cells and thus an increase of cell excitability. In a similar manner, vigilance might increase in response to a release of ACh in response to stress factors such as shock (Zhang et al. 2004), even when bottom-up and top-down signals have a good match based on similarity alone.

Other models have considered alternative effects of ACh modulation. For example, the model of primary auditory cortex by Soto et al. (2006) includes only a single AHP current, but also considers the effect on sodium currents (Cantrell and Catterall 2001) and ACh synaptic modulation which effectively changes network connectivity (Hsieh et al. 2000). Finally, Wang et al. (2003) have included a Na^+-dependent K^+ current and a Ca^{2+}-dependent K^+ current into their model of cells in primary visual cortex to explain adaptation on two different timescales.

These AHP currents differ both in degree of modulation and the underlying mechanism of modulation. There still remains no consensus on what is the composite of channels supporting each of these currents, and there remain discrepancies in the observed effects of pharmacological agents, as well as variations in both channel and current naming schemes (Lima and Marrion 2007; Sah 1996; Villalobos et al. 2004; Wei et al. 2005). Nonetheless, results show that application of acetylcholine and muscarinic agonists reduces or abolishes the sAHP in a variety of tissue types and species (Klink and Alonso 1997; Lorenzon and Foehring 1992; McCormick

and Williamson 1989; Muller et al. 1992; Pedarzani and Storm 1996; Schwindt et al. 1988b). Findings for the cholinergic modulation of the mAHP current are mixed, but generally show a reduction in mAHP conductance to about 70% by applying muscarinic agonists (Lorenzon and Foehring 1992; Power and Sah 2008; Shapiro et al. 2000; Storm 1989). Experiments on the cholinergic modulation of the fAHP current have produced more conflicting results. Cholinergic agonists either cause fAHP increase (Bordey et al. 2000; Kong et al. 2005), no change in fAHP (Lorenzon and Foehring 1992; Storm 1987), or affect fAHP depending on the membrane potential, but probably causes increase under normal conditions (Akins et al. 1990; Cox et al. 1997; Hicks and Marrion 1998; Kong et al. 2007; Nakajima et al. 1986; Schreiber and Salkoff 1997). These physiological findings are described in further detail and compared with model parameters in Section 2.

The current article builds upon these previous analyses and findings to demonstrates how the collective state of the three AHP conductances can control the shape of a sigmoidal transfer function by independently translating its threshold and changing its slope. The analysis reveals simple rules that govern how *parametric space* of cell membrane conductances can be mapped onto the *operational space* of cell signaling, as described by threshold, slope and asymptote of the transfer function to generate desired changes in signaling. By including a combination of three AHP currents, each uniquely modulated by ACh, we examine specific effects that are alternative to a simple gain in cell excitability, namely that ACh may predominantly cause a translation of the threshold of the sigmoidal transfer function.

Section 2 describes the differential equations for the compartmental spiking neuron model, the physiological basis of the simulation parameters, the AHP modeling with spike-dependence and with calcium dynamics, synaptic modeling, the relation between parametric and operational spaces, estimation of cholinergic behavioral intensities, and general analysis techniques. Section 3 describes simulation results, and provides a comparison between the basal sigmoidal transfer functions for different synaptic models, the conservation laws of the function's asymptote, parametric operations for threshold translation and slope change with an assessment of the linearity of these operations, and finally an evaluation of the effect of acetylcholine on cell behavior. Section 4 discusses the significance of the work within the context of learning and behavior.

2 Experimental Procedures

2.1 Compartmental spiking model

Simulated neurons are composed of three cylindrical compartments: somatic, proximal dendritic and distal dendritic. Compartment membrane equations are governed by Hodgkin-Huxley or conductance-based dynamics (Hodgkin and Huxley 1952). The somatic membrane potential, V_S, fluctuates via spike-generating sodium and potassium currents, leak current, dendritic inter-compartmental current, and three AHP currents, with the respective terms in Eq. (1):

$$C_M \frac{dV_s}{dt} = I_{Na} + I_K + I_L + I_{Ca} + I_{fAHP} + I_{mAHP} + I_{sAHP} + \frac{d_s g_a}{4l_s^2}(V_p - V_s) \quad (1)$$

where the first three currents use the Hodgkin-Huxley form (Hodgkin and Huxley 1952):

$$I_{Na} = g_{Na} m_{Na}{}^3 h_{Na}(E_{Na} - V), \quad (2)$$

$$I_K = g_K n_K{}^4 (E_K - V), \quad (3)$$

and

$$I_L = g_L(E_L - V), \tag{4}$$

with "shunting" terms $(E - V)$ in each current. Table 1 lists the complete names, units, and values for the parameters and the previous studies on which they are based.

Table 1 Basic model parameters

Compartment	Parameter Name	Variable	Value(s)	Reference
Somatic	Membrane capacitance	C_M	1 µF/cm²	(Hodgkin and Huxley, 1952)
	Sodium conductance	g_{Na}	45 mS/cm^2	Adjusted to be stable at rest
	Sodium equilibrium potential	E_{Na}	50 mV	(Grossberg and Versace, 2008)
	Potassium conductance	g_K	16 mS/cm^2	Adjusted to be stable at rest
	Potassium equilibrium potential	E_K	-100 mV	(Lee et al, 2005)
	Leak conductance	$g_{L,s}$	0.1 mS/cm^2	(Traub et al., 1991)
	Leak equilibrium potential	E_L	-65 mV	(Storm, 1987)
	Diameter	d_s	0.1 mm	(Grossberg and Versace, 2008)
	Length	l_s	0.15 mm	
	Axial conductance	g_A	0.28 pS	Adjusted to be stable at rest
	AHP Parameters	See Tables 1, 2 & 3		
Proximal Dendrite	Leak conductance	$g_{L,p}$	0.03 mS/cm^2	(Grossberg and Versace, 2008)
	Leak equilibrium potential	E_L	-65 mV	(Storm, 1987)
	Diameter	d_P	0.06 mm	(Grossberg and Versace, 2008)
	Length	L_p	0.4 mm	
	Axial conductance	g_A	0.28 pS	Adjusted to be stable at rest
Distal Dendrite	Leak conductance	$g_{L,d}$	0.03 mS/cm^2	(Grossberg and Versace, 2008)
	Leak equilibrium potential	E_L	-65mV	(Storm, 1987)
	Diameter	d_d	0.06 mm	(Grossberg and Versace, 2008)
	Length	l_d	0.5 mm	
	Axial conductance	g_A	0.28 pS	Adjusted to be stable at rest
	AMPA peak conductance	g_{AMPA}	2.5 or 0.1 pS	Scaled for stimulation rate
	AMPA equilibrium potential	E_{AMPA}	0 mV	(Destexhe et al., 1994a)
	AMPA rise time	$\tau_{r,AMPA}$	0.76 ms	(Povysheva et al. 2006)
	AMPA fall time	$\tau_{f,AMPA}$	6.5 ms	

The somatic sodium and potassium equilibrium potentials and the axial conductance are similar to parameters for layer 5 cells from Grossberg and Versace (2008), but are adjusted such that the cells do not fire at rest, yet are still responsive to stimulation. The dynamics of AHP currents are a function of generated spike history, H_S, and individual rise and fall times, τ_r and τ_f, and are described further in Section 2.3. Activation and inactivation functions, including m_{Na}, h_{Na} and n_K in (2) and (3), follow the conventional form of forward and backward rates, α and β, for voltage-

dependent conductances commonly used for spiking models (Grossberg and Versace 2008; Hodgkin and Huxley 1952; Traub et al. 1991) and each change as x in the equation:

$$\frac{dx}{dt} = \alpha_x(1-x) - \beta_x, \tag{5}$$

or, alternatively, in the equivalent equation:

$$\frac{dx}{dt} = \tau_x(x_{Eq} - x). \tag{6}$$

where specific expressions for α, β, τ and x_{Eq} are listed in Table 2.

Table 2 Activation and Inactivation Equations

Current	Variable, x	Forward Rate, α_x	Backwards Rate, β_x	Reference
Na	m_{Na}	$\dfrac{0.32(13-V)}{e^{0.25(13-V)}-1}$	$\dfrac{-0.28(40-V)}{e^{-0.2(40-V)}-1}$	(Hodgkin and Huxley 1952)
	h_{Na}	$0.128e^{\frac{(17-V)}{18}}$	$\dfrac{4}{e^{0.2(40-V)}+1}$	
K	n_K	$\dfrac{0.032(15-V)}{e^{0.2(15-V)}-1}$	$0.5e^{\frac{(10-V)}{40}}$	
A	m_A	$\dfrac{0.125}{e^{(-28-V)/22.5}+1}$	$\dfrac{0.0625}{e^{(52.8+V)/19.7}+e^{-(82.7+V)/38.7}}$	(Traub et al. 2003; Barkai and Hasselmo 1994)
	h_A	$\dfrac{0.125}{e^{(85+V)/16}+1}$	1.2	
M	m_M	$\dfrac{0.002}{e^{0.2(-25-V)}+1}$	$0.001e^{(-45-V)/6}$	
SK, SK2	p_{SK}, p_{SK2} $c_1 \leftrightarrow c_2$	$200\,[Ca]$	0.08	(Solinas et al., 2007; Hirschberg et al., 1998)
	$c_2 \leftrightarrow c_3$	$160\,[Ca]$	0.08	
	$c_3 \leftrightarrow c_4$	$80\,[Ca]$	0.2	
	$c_3 \leftrightarrow o_1$	0.16	1	
	$c_4 \leftrightarrow o_2$	1.2	0.1	

Current	Variable	Steady State, x_{Eq}	Time, τ	Reference
Ca$_L$, Ca$_N$	m_{LCa}, m_{NCa}	$\dfrac{1}{(1+e^{(-20-V)/5})}$	$1.25\sec h(-0.031(V+37.1))$	(Brown et al. 1993)
	h_{LCa}, h_{NCa}		420	
Ca$_P$	m_{PCa}	$\dfrac{1}{(1+e^{(-18-V)/5.5})}$	$1.25\sec h(-0.031(V+37.1))$	
	h_{PCa}		420	
BK	p_{BK}	$\dfrac{1}{1+1806(\dfrac{1+[Ca]/18.06}{1+[Ca]/2.16})^4 e^{-12.65V}}$	5	(Cox et al. 1997)

Dendritic compartments are passive with leak currents, and are divided into proximal and distal compartments. Inputs are received via an alpha-amino-3-hydroxy-5-methyl-4-isoxazolepropionic acid (AMPA) synaptic current into the distal dendrite and described further in Section 2.6. This

9

dendritic structure allows for dendritic integration of excitatory synaptic input. Proximal and distal dendritic membrane potentials, V_p and V_d, follow Eq. (7) and (8), respectively:

$$C_M \frac{dV_p}{dt} = I_L + \frac{d_p g_a}{4l_p^2}(V_s - V_p) + \frac{d_p g_a}{4l_p^2}(V_d - V_p) \tag{7}$$

and

$$C_M \frac{dV_d}{dt} = I_L + \frac{d_d g_a}{4l_d^2}(V_p - V_d) + I_{AMPA} \tag{8}$$

with the parameters defined in Table 1.

2.2 Modeling spike-dependent signals

An individual excitatory postsynaptic potential (EPSP) occurs as a time-varying conductance wave after each arriving presynaptic (or input) spike, while an after-hyperpolarization (AHP) current results from a time-varying conductance wave after each postsynaptic (or output) spike. Given a single spike occurring at time t_s, a double exponential function for a conductance g_E describes both its onset and decay:

$$g_E(t, \tau_r, \tau_f, t_s) = c(e^{-(t-t_s)/\tau_f} - e^{-(t-t_s)/\tau_r}), \tag{9}$$

where τ_r and τ_f are rise and fall time constants respectively (Destexhe et al. 1994a). For a single spike, the conductance peaks at time t_{peak},

$$t_{peak} = \frac{\tau_r \tau_f}{\tau_f - \tau_f} \ln(\frac{\tau_r}{\tau_f}), \tag{10}$$

with an amplitude of 1, ensured by the normalizing constant c,

$$c = \frac{1}{(\frac{\tau_r}{\tau_f})^{\tau_r/(\tau_f - \tau_r)} - (\frac{\tau_r}{\tau_f})^{\tau_f/(\tau_f - \tau_r)}}. \tag{11}$$

A spike train, whether input or output signals, defines a history, or list, H, of spike times:

$$H(t) = \{t_1, .. t_N\}. \tag{12}$$

Output spikes, H_s, are determined by when the somatic potential, V_s, crosses a detection threshold, $V_{th} = 10$mV, with a negative derivative (a positive derivative produces similar results). A spike history poses the problem of conductance saturation during temporal summation. We consider three spike-dependent models, which exhibit different behavior during temporal summation: .

Total conductance could be unbounded, accumulating at the same rate regardless of how many spikes occur over an interval. This approach is equivalent to summing up independent double exponentials for each spike represented by Eq. (9). A discrete algorithm that leverages z-transform mathematics can efficiently compute the sum of these double exponential waveforms (Kohn and Worgotter 1998). The algorithm solves the computation with a discrete form of the signal by converting time t into n discrete steps of duration T (we use 0.02 ms):

$$g_{IE}(t, \tau_r, \tau_f, H) = g_{IE}(nT, H) = g_{IE}(n), \tag{13}$$

such that the total conductance can be computed in a recursive fashion,

$$g_{IE}(n) = (a_r - a_f)H(n-1) + (a_r + a_f)g_{IE}(n-1) - a_r a_f g_{IE}(n-2), \tag{14}$$

10

where $a_r = e^{-T/\tau_r}$ and $a_f = e^{-T/\tau_f}$ and *H(n-1)* denotes whether there was a spike at the last time step. We refer to this as the *independent exponentials (IE)* spike-dependent signal.

Alternatively, a total conductance could be strictly bounded no matter how many spikes occur over an interval. This limited capacity may be approximated adding the conductances computed from the previous two spike times, t_1 and t_2, and subtracting their product:

$$g_{NE}(t, \tau_f, \tau_f, H) = g_E(t, t_1) + g_E(t, t_2) - g_E(t, t_1)g_E(t, t_2). \tag{15}$$

We refer to this as the *normalized exponentials (NE)* spike-dependent signal, introduced by KInNeSS, the KDE Integrated NeuroSimulation Software environment (Versace et al. 2008).

A more realistic approximation uses a mass action law, similar to other kinetic models (Destexhe et al. 1994a, 1994b), to introduce an intermediate variable. This is expressed by two differential equations:

$$\frac{dR}{dt} = (1 - R)I - \frac{R}{\tau_r}, \tag{16}$$

and

$$\frac{dg_{SD}}{dt} = (\frac{\tau_f + \tau_r}{\tau_f})[\frac{2}{\tau_r}(1 - g_{SD})R - \frac{g_{SD}}{\tau_f}]. \tag{17}$$

For a synaptic signal, this new variable *R* most closely portrays the concentration of transmitter in the cleft, while the conductance g_{SD} represents postsynaptic receptor activation. The function *I* denotes the input signal, a set of square waves from the spike train, *H*, which equals $1/\tau_r$, if the time since the last spike arrival, $t - t_n$, is less than τ_r ms, and equals 0 otherwise. The passive decay rate parameters, $1/\tau_r$ and $1/\tau_f$, can be thought of as the diffusion rate of the neurotransmitter and as the average dissociation rate of the neurotransmitter from the receptors, respectively. The net conductance change following a single presynaptic spike resembles the double exponential wave in Eq. (9) (as noted in Fig. 2(a)). This formalism implies that the conductance does not saturate after a single spike, but does approach a saturation level given a prolonged high firing rate or a rapid burst of spikes. For this reason, it is the preferred form for both strong driving synapses and for AHP currents. We refer to it as the *saturating differentials (SD)* spike-dependent signal.
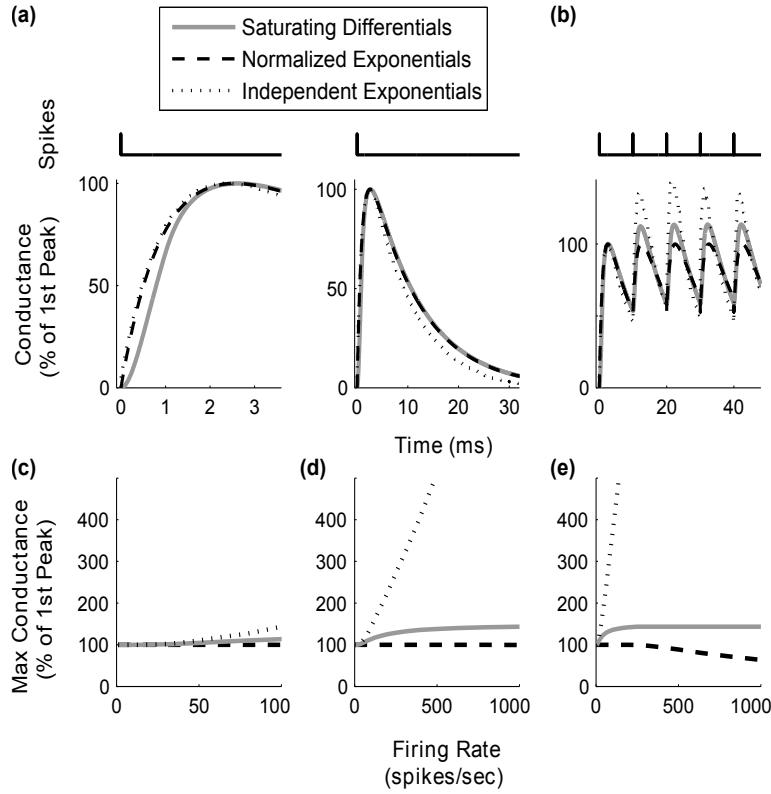
Fig. 2 Spike-dependent signals. (**a**) Individual conductance waves as a percentage of first peak conductance where $\tau_r = 1$ms and $\tau_f = 10$ms, compared for the three spike-dependent models (*saturating differentials*, *normalized exponentials*, and *independent exponentials*). (**b**) Conductance waves as in (a) with a stimulation rate of 100 spikes/sec. Synaptic models are distinguished by temporal summation starting with the 2nd spike. (**c,d**) Maximal conductance over 2000 ms as a percentage of the first peak conductance with spike trains up to (**c**) 100 spikes/sec and (**d**) 1000 spikes/sec (**e**) Maximal conductance as a percentage of the first peak conductance with slower time constants $\tau_r = 10$ms and $\tau_f = 100$ms

2.3 Modeling spike-based after-hyperpolarization currents

Since fluctuations in somatic calcium concentrations strongly match the timing of action potentials, and after-hyperpolarization (AHP) currents are predominantly carried by calcium-dependent potassium channels (Abel et al. 2004; Lancaster and Adams 1986; Lee et al. 2005; Prakriya et al. 1996), these currents are spike-dependent. For the *spike-based AHP* cell model, individual AHP currents are modeled by a wave of increased conductance following each spike, as in Eq. (9), and follow the equations:

$$I_{fAHP} = g_{fAHP}g_{SD}(t,\tau_{r,fAHP},\tau_{f,fAHP},H_s)(E_{fAHP}-V_S)\,, \tag{18}$$

$$I_{mAHP} = g_{mAHP}g_{SD}(t,\tau_{r,mAHP},\tau_{f,mAHP},H_s)(E_{mAHP}-V_S)\,, \tag{19}$$

and

$$I_{sAHP} = g_{sAHP}g_{SD}(t,\tau_{r,sAHP},\tau_{f,sAHP},H_s)(E_{sAHP}-V_S)\,. \tag{20}$$

Since each AHP current within an individual cell has a bounded conductance based, say, on channel density, then during summation across the spiking history, this bound must be enforced. Therefore, the spike-dependent signals in Eqs. (18)-(20), take the *saturating differentials* form of Eqs. (16) and (17) for their time course.
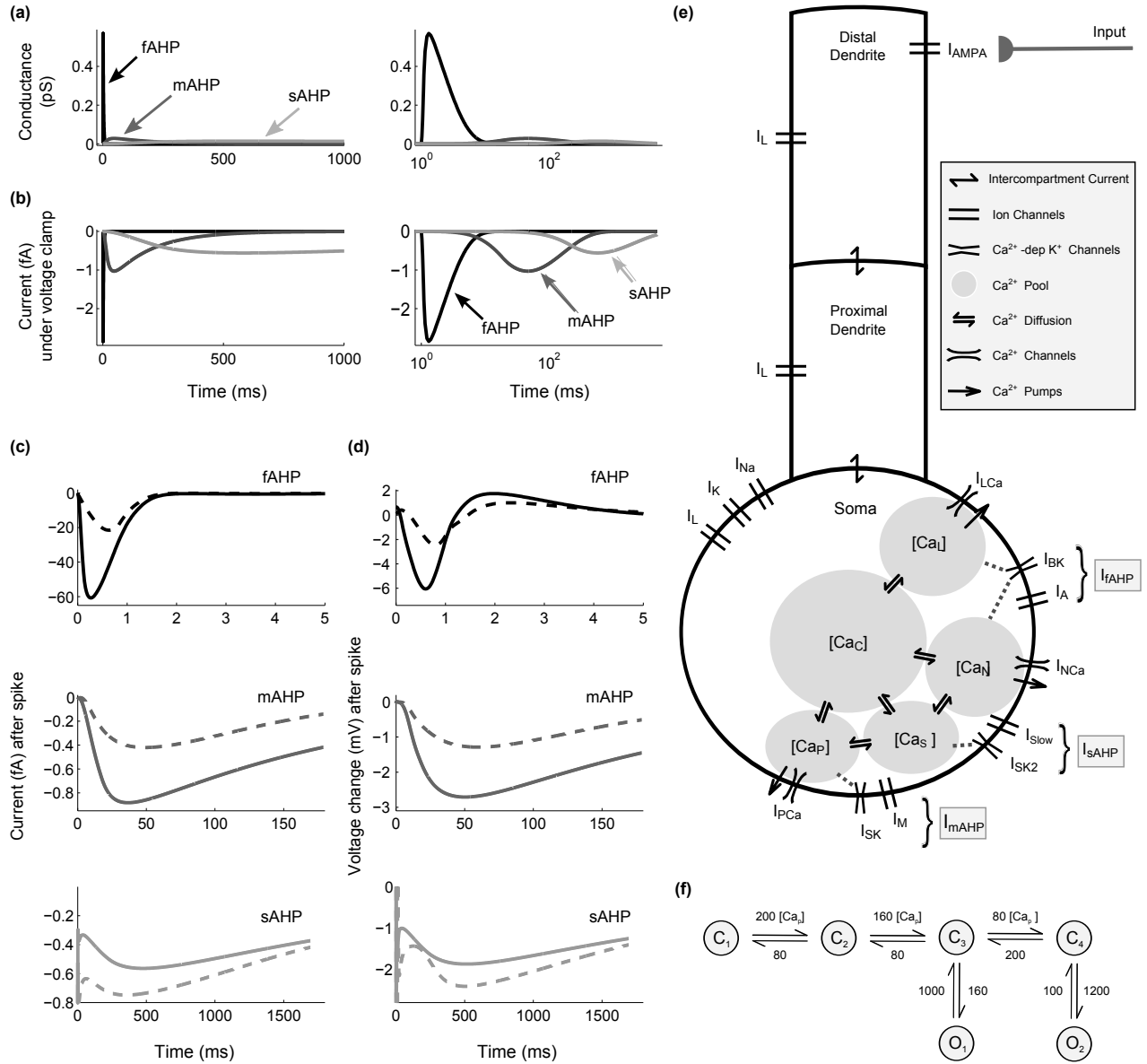
The parameters for the model match measurements observed in mammalian neocortex by Lee et al. (2005) and Storm (Storm 1987), and were selected because of the experimental specificity provided by their studies (Table 3). Fig. 3a depicts the magnitude of the three AHP conductances over 1000ms following a spike on linear and logarithmic scales and currents. Fig. 3b depicts the three AHP currents induced by a single spike with a voltage clamp holding at -60mV. These basal levels were determined by measuring the amplitude difference in somatic potential, V_s, between simulation of individual spikes with and without each AHP current, as

12

shown in Fig. 3c-e, and then changing conductances using a method of guess-and-check until amplitudes approximately matched measurements from physiological studies (Table 3).

Table 3 Comparison of physiological AHP data with basal model parameters

Current	Model or tissue, species		Conduct[c] g_{AHP} (pS)	Equil[b] E_{AHP} (mV)	Amplitude (mV)	Rise τ_r (ms)	Fall τ_f (ms)	TTP[a] (ms)	References
fAHP	Spike-based		0.8	-65	6.7	0.1	2.0	0.6	n/a
	Ca-based	BK	0.9	-65	3.2	n/a	n/a	0.8	n/a
		A	0.98	-80					
	Rat Hippocampus		n/a	-65	7	n/a	2-5	0.9	(Storm, 1987)
	Human Neocortex		n/a	-65	n/a	n/a	n/a	n/a	(Lorenzon and Foehring 1992)
	Cat Sensorimotor		n/a	-71	10	n/a	n/a	n/a	(Schwindt et al. 1988a)
mAHP	Spike-based		0.04	-97	2.7	18	164	50	n/a
	Ca-based	SK	0.032	-97	1.3	n/a	n/a	60	n/a
		M	0.036	-97					
	Rat Neocortex		n/a	-97	5.3	18	164	60	(Lee et al, 2005)
	Human Neocortex		n/a	-93	1.6	n/a	38-60	n/a	(Lorenzon and Foehring 1992)
	Cat Sensorimotor		n/a	-100	n/a	n/a	n/a	112	(Schwindt et al. 1988a)
sAHP	Spike-based Cell		0.02	-100	1.9[d]	225	2200	514	n/a
	Ca-based Cell	SK2	0.0156	-100	2.4[d]	n/a	n/a	502	n/a
		SL	0.0172	-100					
	Rat Neocortex		n/a	-100	7.5[d]	225	3691	926	(Lee et al, 2005)
	Cat Sensorimotor		n/a	-99	2.5[d]	n/a	n/a	774	(Schwindt et al. 1988a,b)
	Human Neocortex		n/a	-87	1.8[d]	n/a	687-999	n/a	(Lorenzon and Foehring 1992)

[a] TTP = Time to peak; [b]Equil = Equilbrium; [c]Conduct = Conductance, [d]After 10 spikes

(a) fAHP mAHP sAHP

Conductance (pS)

0.4 0.2

(b) Current (fA) under voltage clamp

fAHP mAHP sAHP

Time (ms)

(c) Current (fA) after spike

fAHP
mAHP
sAHP

Time (ms)

(d) Voltage change (mV) after spike

fAHP
mAHP
sAHP

Time (ms)

(e)

Distal Dendrite — I_{AMPA} — Input

I_L

Proximal Dendrite

I_L

Intercompartment Current
Ion Channels
Ca^{2+} -dep K^+ Channels
Ca^{2+} Pool
Ca^{2+} Diffusion
Ca^{2+} Channels
Ca^{2+} Pumps

I_{Na} I_K I_L Soma I_{LCa}

$[Ca_L]$ $[Ca_C]$ $[Ca_N]$ $[Ca_P]$ $[Ca_S]$

I_{BK} I_A } I_{fAHP}

I_{NCa}

I_{Slow} I_{SK2} } I_{sAHP}

I_{PCa} I_{SK} I_M } I_{mAHP}

(f)

$C_1 \underset{80}{\overset{200\,[Ca_a]}{\rightleftharpoons}} C_2 \underset{80}{\overset{160\,[Ca_a]}{\rightleftharpoons}} C_3 \underset{200}{\overset{80\,[Ca_a]}{\rightleftharpoons}} C_4$

$C_3 \underset{160}{\overset{1000}{\rightleftharpoons}} O_1$ $C_4 \underset{1200}{\overset{100}{\rightleftharpoons}} O_2$

Fig. 3 Modeling of AHP physiology. (**a**) AHP conductances and (**b**) current under voltage clamp at -60mV from the *spike-based* AHP cell model displayed on a linear scale and on a logarithmic scale. (**c**) Current following a single spike for fAHP and mAHP currents, and following 10 spikes for sAHP current. Results shown for *spike-based* (solid line) and *calcium-based* (dashed line) AHP models. (**d**) Effect on membrane voltage following a spike (difference between with and without the AHP current) for fAHP and mAHP, and following 10 spikes for sAHP. (**e**) Diagram of the *calcium-based* AHP cell model, dotted lines indicate calcium dependence of AHP channels. (**f**) Small conductance potassium (SK) channel sequential transition where numbers express transition rates in ms

14

2.4 Modeling after-hyperpolarization currents with calcium dynamics

Another cell model is also considered, in which AHP currents are controlled partly by calcium dynamics. Instead of the spike-dependent AHPs, described by (18)-(20), the specific physiological channels are introduced. Here, calcium channels cause local calcium influx during spikes that mediates the calcium-dependent portion of AHP currents. Fig. 3e depicts all the components of this *calcium-based AHP* cell model.

     Calcium Currents. Somatic calcium current is composed of three calcium currents types, L-type, N-type and P-type, which occur roughly in equal proportion in cortical cells (Lorenzon and Foehring 1995):

$$I_{Ca} = I_{LCa} + I_{PCa} + I_{NCa}. \tag{21}$$

The underlying channel structures have since been identified and labeled $Ca_V1.3$, $Ca_V2.2$, and $Ca_V2.1$, respectively. T-type calcium currents are excluded from the model, because they are observed in bursting, not regular, firing neurons. Q-type and R-type are excluded, because information about these currents in cortex is scarce and they appear not to contribute significantly to Ca^{2+} current in neocortical cells. All three currents follow the same form:

$$I_{LCa} = g_{LCa} m_{LCa} h_{LCa} g_{GHK}(V_s, [Ca_L]), \tag{22}$$

$$I_{NCa} = g_{NCa} m_{NCa} h_{NCa} g_{GHK}(V_s, [Ca_N]), \tag{23}$$

and

$$I_{PCa} = g_{PCa} m_{PCa} h_{PCa} g_{GHK}(V_s, [Ca_P]). \tag{24}$$

The GHK (Goldman-Hodgkin-Katz) current equation (Goldman 1943; Hodgkin and Katz 1949) is employed, rather than the previous Hodgkin & Huxley form, to capture that these currents are sensitive to internal calcium, notably such that calcium current decreases with increased internal calcium:

$$g_{GHK}(V_s, [Ca]) = -0.213 V_s \frac{[Ca] - [Ca_o] e^{-0.0325V}}{1 - e^{-0.0325V}}, \tag{25}$$

where the internal calcium concentration, $[Ca_o]$, is set to 5 mM as per Lorenzon and Foehring (1995). The L-type, N-type and P-type currents differ in the voltage threshold of activation and in their inactivating properties. Activation and inactivation equations, shown in Table 2, are derived from measurements of pyramidal cells in sensorimotor neocortex (Brown et al. 1993), and correspond to other studies on calcium currents (Anwar et al. 2010; Delcour et al. 1993; King and Meriney 2005; Lorenzon and Foehring 1995; Luvisetto et al. 2004; Wilson et al. 2004).

     Calcium Dynamics. Each AHP current exhibits a different dependence on these calcium sources. This calcium-dependent specificity of AHP currents was noted for mAHP and sAHP by Pineda et al. (1998) and for fAHP by Sun et al. (2003) and Loane et al. (2007). To capture this specificity, the model includes local somatic calcium concentrations near sources and a cytosolic calcium concentration. The model of calcium dynamics is based on previous models (Anwar et al. 2010; Barkai and Hasselmo 1994; Canavier et al. 2007; Wang et al. 2003; Wilson et al. 2004). The cytosolic calcium, $[Ca_C]$ in mM, follows the equation:

$$\frac{d[Ca_C]}{dt} = b_c([Ca_R] - [Ca_C]) + \delta_c([Ca_L] - [Ca_C]) +$$

$$\delta_c([Ca_N] - [Ca_C]) + \delta_c([Ca_P] - [Ca_C]) + \delta_S([Ca_S] - [Ca_C]), \tag{26}$$

which tends toward a resting calcium concentration, $[Ca_R] = 10^{-6}$ mM = 1 nM (Abel et al. 2004; Anwar et al. 2010; Lorenzon and Foehring 1995), at a rate, $b_c = 1/(80$ ms$)$. The diffusion rate, δ_C

= 1/(800ms), defines the exchange rate between the other calcium concentration pools. Local calcium concentrations, also in mM, are coupled to specific calcium channel (L-, N-, P-type):

$$\frac{d[Ca_L]}{dt} = fI_{LCa} - \alpha_L[Ca_L] + \delta_C([Ca_C] - [Ca_L]), \tag{27}$$

$$\frac{d[Ca_N]}{dt} = fI_{NCa} - \alpha_N[Ca_N] + \delta_C([Ca_C] - [Ca_N]) + \delta_S([Ca_S] - [Ca_N]), \tag{28}$$

and

$$\frac{d[Ca_P]}{dt} = fI_{PCa} - \alpha_P[Ca_P] + \delta_C([Ca_C] - [Ca_P]) + \delta_S([Ca_S] - [Ca_P]) \tag{29}$$

where $f = 0.002$ M/(pA*ms) scales influx from channels (Wang et al. 2003), and the rates $\alpha_L = 1/(120ms)$, $\alpha_N = 1/(360ms)$, $\alpha_P = 1/(160ms)$ describe the speed of calcium removal by membrane pumps. Cytosolic calcium diffuses gradually into a slow calcium concentration pool, posited to be near sAHP channels:

$$\frac{d[Ca_S]}{dt} = \delta_S([Ca_C] - [Ca_S]) + \delta_S([Ca_N] - [Ca_S]) + \delta_S([Ca_P] - [Ca_S]) \tag{30}$$

with a slower diffusion rate $\delta_S = 1/(3600ms)$.

AHP Currents. AHP currents are predominantly calcium-dependent potassium currents (Hotson and Prince 1980; Lancaster and Adams 1986), but also partly calcium-independent voltage potassium currents (Lorenzon and Foehring 1992). Thus, each AHP current consists of a Ca-dependent and Ca-independent term.

Fast AHP. The calcium-dependent portion of the fAHP is called the BK current (for Big conductance potassium current):

$$I_{fAHP} = I_{BK} + I_A, \tag{31}$$

and depends on influx from L-type and N-type channels (Sun et al. 2003; Loane et al. 2007):

$$I_{BK} = g_{BK}p_{BK}([Ca_L] + [Ca_N], V_s)(E_{BK} - V_s). \tag{32}$$

Equations for its calcium-dependence are detailed by Cox et al. (1997) based on analysis of physiological recordings and used by Anwar et al. (2010). We also employ their equations (see Table 2). The transient current, called the "A" current, is believed to constitute the calcium-independent portion of the fAHP current. The equation for the A current follows other models (Barkai and Hasselmo 1994; Rhodes and Gray 1994; Traub et al. 2005, 2003):

$$I_A = g_A m_A^4 h_A (E_A - V_s). \tag{33}$$

Medium AHP. The calcium-dependent portion of the mAHP is called the SK current (for Small conductance potassium current):

$$I_{mAHP} = I_{SK} + I_M. \tag{34}$$

We use a state-based gating scheme derived from cloned rat SK channels (Hirschberg et al., 1998), but modified to be based on the specific P-type calcium pool, $[Ca_P]$ (Pineda et al. 1998):

$$I_{SK} = g_{SK}p_{SK}([Ca_P], V_s)(E_{SK} - V_s). \tag{35}$$

The gating p_{SK} is the percentage of channels in the open state, $O_1 + O_2$, based on the sequential transition scheme, depicted in Fig. 3f. The channel population is originally set to the lowest closed state ($C_1 = 1$, other states = 0). This channel scheme has also been used in other models (Anwar et al. 2010; Traub et al. 2005, 2003).

A potassium current, called the "M" current (for Muscarinic), is thought to constitute the calcium-independent portion of the mAHP. The equation for this current is based on other models (Barkai and Hasselmo 1994; Rhodes and Gray 1994; Traub et al. 2005, 2003):

$$I_M = g_M m_M (E_M - V_s). \tag{36}$$

Slow AHP. The calcium-dependent portion of the sAHP might also be carried by SK, though this has been debated (Abel et al. 2004). We use the same SK equations as for the mAHP, except that it is dependent on the slow calcium pool, $[Ca_S]$, rather than $[Ca_p]$ (Pineda et al. 1998):

$$I_{sAHP} = I_{SK2} + I_{SL}, \tag{37}$$

and

$$I_{SK2} = g_{SK2} p_{SK2} ([Ca_S], V_s)(E_{SK2} - V_s). \tag{38}$$

An unknown current constitutes the calcium independent component of sAHP, so it is treated as spike-dependent:

$$I_{SL} = g_{SL} g_{SD}(t, \tau_{r,SL}, \tau_{f,SL}, H_s)(E_{SL} - V_s), \tag{39}$$

where $\tau_{r,SL} = 225$ms and $\tau_{f,SL} = 2400$ms. The conductances of each AHP channel, and the calcium pump and diffusion rates in this *calcium-based* cell model were adjusted until the time course and magnitude of each AHP roughly matched those for the *spike-based* cell model. Figs. 3c,d compare the three AHPs of the two models with their voltage and current traces.

2.5. Modeling acetylcholine modulation

We estimate the different intensities of cholinergic modulation that correspond to behavioral or attentional states by examining an array of experiments. These studies, displayed in Table 5, estimate the concentrations and relative magnitudes of ACh release for different states. The majority of the studies used a microdialysis technique to measure the concentration of neurotransmitter, a technique known to salvage only between 5-20% of the original concentration. When recovery percentages are reported, we adjusted these estimates to compensate for this limitation by dividing the reported concentration by the recovery percentage to estimate the original concentration.

The novel technique of using choline-sensitive microelectrodes has produced data with high temporal resolution showing rapid increases in ACh during a presented cue (Parikh et al. 2007). To convert these results from transients above the mean into percentage changes for comparison with other studies, we assumed (1) that basal ACh concentrations in Parikh et al. (2007) are close to measurements in Parikh and Sarter (2006) with the same rat species, methodology, and lab; and (2) that the ratio of actual ACh concentration to measured extracellular choline concentration is about 0.083 (340 μM / 4110 μM) based on a related study (Köppen et al. 1996). This calculation parallels that made for microdialysis with recovery percentages. For both experimental techniques, we do not expect measurements to be precise. Nor do we note any significant conformity between the two. Rather, we are concerned with relative fluctuations.

Table 4 Pharmacological modulation of AHP currents by ACh receptor agonists

Current	% of Basal	Magnitude		Pharmacological		Species Tissue	References
		Before (mV)	After (mV)	Agent	Con[d] (μM)		
fAHP	150%	6.7	10.1	ACh	1	Model	n/a
	n/a	n/a	22 pA, 78 pA, 197 pA	ACh	2.5, 10, 100	Guinea Pig Vestibular Hair Cells	(Kong et al. 2005)
	n/a	n/a	650 pA	ACh	200	Human Astrocytes	(Bordey et al. 2000)
	No Effect	n/a	n/a	Carbachol (Muscarinic)	50	Human Neocortex	(Lorenzon and Foehring 1992) (Storm 1989)
	260%	5097 pA	13232 pA	Muscarine	50	Rat Chromaffin Cells	(Prakiya et al. 1996)
	133%	520 pA	690 pA	Carbachol, -90mV	100	Rat Neostriatal	(Akins et al. 1990)
	72%	720 pA	520 pA	Carbachol, -60mV	100		
	160%	150 pA	240 pA	ACh, -75mV	0.1	Rat Hippocampus	(Nakajima et al. 1986)
	67%	450 pA	300 pA	ACh, -44mV	0.1		
mAHP	80%	2.7	2.2	ACh	1	Model	n/a
	55%	7.3	4.0	Muscarine	10	Human Neocortex	(Lorenzon and Foehring 1992)
	50%	8.0	4.0	Carbachol	30	Rat mPFC	(Satake et al. 2008)
	72%	3.6	2.6	Carbachol	40	Rat Hippocampus	(Storm 1989)
	No Effect	n/a	n/a	Muscarine	5	Cat Sensorimotor	(Schwindt et al. 1988b)
	100%	8.0	8.0	Carbachol	50	Rat Entorhinal	(Klink and Alonso 1997)
sAHP	30%	1.9	0.6	ACh	1	Model	n/a
	33%	3.0	1.0	Muscarine	10	Human Neocortex	(Lorenzon and Foehring 1992)
	89%	7	6.2	Carbachol	0.3	Rat mPFC	(Satake et al. 2008)
	51%		3.6		3		
	-3%		-0.2		30		
	0%	3.0	0.0	Muscarine	5	Cat Sensorimotor	(Schwindt et al., 1988b)
	11%	4.5	0.5	Carbachol	50	Rat Entorhinal	(Klink and Alonso, 1997)

[d]Con = Concentration

We also estimate the impact of increasing the cholinergic intensity on the AHP currents by examining an array of physiological studies. The physiology has shown that these AHP currents differ both in degree of modulation and the underlying mechanism of modulation.

Slow AHP data. Results for the sAHP modulation show that application of acetylcholine and muscarinic agonists reduces or entirely abolishes sAHP (Table 4). The mechanism of cholinergic modulation of sAHP occurs indirectly via muscarinic receptors mediated either

partly by Ca^{2+}/calmodulin-dependent protein kinase II (Muller et al. 1992; Pedarzani and Storm 1996) or by a guanine nucleotide binding protein (or G protein) engaging with an unknown phosphatase (Krause and Pedarzani 2000).

Medium AHP data. Findings for the cholinergic modulation of the mAHP current are mixed. Schwindt and colleagues (Schwindt et al. 1988b) observed no effect on mAHP with an application of 5 μM of muscarine to cat cortical cells. However, later experiments showed a partial reduction of mAHP conductance to about 70% of its basal value by applying either 10 μM muscarine in human neocortex (Lorenzon and Foehring 1992) or 40 μM carbachol in rat hippocampus (Storm 1989). The mAHP current is considered to be carried mainly by SK calcium-dependent potassium channels, which are generally distinguished by their sensitivity to blockade by apamin. Recent findings showed that focal application might enhance the mAHP conductance in rat amygdala by boosting intracellular calcium, while bath application causes a diminishing of the current (Power and Sah 2008). However, this result uses a novel approach to measure the current under cholinergic stimulation and should be confirmed in other tissue samples by other labs.

Fast AHP data. Experiments on the cholinergic modulation of the fAHP current have produced more conflicting results. Early physiological studies reported no change in fAHP conductance with the application of 50 μM of the muscarinic agonist carbachol, but also fail to provide a figure as evidence for this result (Lorenzon and Foehring 1992; Storm 1987). A variety of later work, albeit mainly non-cortical or non-pyramidal, supports the hypothesis that ACh stimulation causes an increase in fAHP conductance. Stimulation with ACh elevates fAHP current via muscarinic receptors in cancerous astrocytes of human neocortex (Bordey et al. 2000) and amplifies fAHP currents via nicotinic receptors in vestibular hair cells of pigs (Kong et al. 2005). Similarly, in rat sympathetic neurons, BK channels activate with calcium influx as a result of ACh receptor activation (Prakriya et al. 1996; Prakriya and Lingle 1999). Detailed physiology of BK calcium-dependent potassium channels, the main carriers of the fAHP, has helped to explain the effect. Activation of BK channels depends jointly on the membrane voltage and two binding sites for calcium, one of which is also sensitive to cadmium (Schreiber and Salkoff 1997). Cholinergic stimulation is, thus, presumed to release calcium from internal stores to effectively promote BK channel activation and increased fAHP conductance by causing a depolarizing shift in the voltage-based activation curve. Additionally, BK channels exhibit inactivation, which likewise is jointly voltage- and calcium-dependent, and is believed to be caused by blocking of the channel pore on the intracellular side (Hicks and Marrion 1998), probably by movement of its transmembrane β subunit (Wallner et al. 1999).

A detailed kinetic model, matched with physiological results, has advanced a precise explanation of how increased calcium causes a depolarizing shift in both the activation and inactivation functions (Cox et al. 1997). This implies that cholinergic stimulation raises fAHP conductance in a hyperpolarized membrane, and lowers fAHP conductance in a depolarized membrane. Indeed, this effect has been observed with a 10 μM application of muscarine in rat neostriatum (Akins et al. 1990). The opposite effect has been observed with a 0.1 μM application of acetylcholine in rat hippocampus (Nakajima et al. 1986). Nonetheless, at hyperpolarized membrane voltage near rest, approximately -70mV, it appears that both studies show an increase in fAHP from the modulatory signal. In the vestibular hair cells of the guinea pig, ACh-induced BK currents exhibit a reversal potential of around -65 mV (Kong et al. 2005, 2007). The studies from Kong and colleagues are of particular interest, because they show graded changes in BK current with rising levels of ACh. Taken together, these findings support the hypothesis that ACh

increases fAHP in neocortical pyramidal under normal conditions. The changes in magnitude for each AHP current following application of acetylcholine or cholinergic agonists are summarized quantitatively in Table 4.

Table 5 Behavioral correspondence to cholinergic intensities

Intensity	Behavioral Event	ACh Concentration		Recovery (Dialysis)	Species Tissue	References
		% Basal	Estimate (nM)			
Low	n/a	50%	250	n/a	Model	n/a
	SW Sleep	44%	{150}	n/a	Cat Frontal Cortex	(Marrosu et al. 1995)
	SW Sleep	44%	0.72 {0.16}	22%	Rat Thalamus	(Williams et al. 1994)
	Light phase	70%	33.5	n/a	Rat Hippocampus	(Crouzier et al. 2006)
Basal	n/a	100%	500	n/a	Model	n/a
	None	100%	400[f], 4850[e]	n/a	Rat Frontoparietal	(Parikh and Sarter 2006)
	None	100%	400[f], 4850[e, f]	n/a	Rat PFC	(Parikh et al. 2007)
	None	100%	3.6 {0.29}	>8%		
	None	100%	340, 4110[e]	17%	Rat Hippocampus	(Köppen et al. 1996)
	Wake Quiet	100%	{344}	n/a	Cat Frontal Cortex	(Marrosu et al. 1995)
	None	100%	56 {8.4}	15%	Rat Frontoparietal	(Arnold et al. 2002)
	Wake	100%	1.64 {0.36}	22%	Rat Thalamus	(Williams et al. 1994)
	Dark phase	100%	47.8	n/a	Rat Hippocampus	(Crouzier et al. 2006)
Moderate	n/a	150%	750	n/a	Model	n/a
	Task	137%	550[f], 6650[e,f]	n/a	Rat PFC	(Parikh et al. 2007)
	Task	190%	6.8 {0.55}	>8%		
	Cue-evoked Misses	150%	600[f], 7250[e,f]	n/a		
	Listening to Bird Songs	122%	{420}	n/a	Cat Frontal Cortex	(Marrosu et al. 1995)
	Fixed Interval 9s	140%	78.4 {11.7}	15%	Rat Frontoparietal	(Arnold et al. 2002)
High	n/a	200%	1000	n/a	Model	n/a
	Cue-evoked Detections	182%	730, 8850[e,f]		Rat PFC	(Parikh et al. 2007)
	Sustained Attention	220%	123 {18.5}	15%	Rat Frontoparietal	(Arnold et al. 2002)
Very High	n/a	300%	1500	n/a	Model	n/a

{} Indicate raw micro dialysis values before correction with recovery percentage.
[e] Measurements of choline concentration which imply ACh concentration
[f] Speculated values based on 2 assumptions: (1) that basal ACh concentrations in (Parikh et al., 2007) are close to those from (Parikh and Sarter, 2006) with the same rat species, methodology, and lab, and (2) that the ratio of actual ACh concentration to measured choline concentration is 0.083 (340 μM / 4110 μM) based on (Köppen et al., 1996). See methods for details.

Model AHP hypotheses. Our model assumes ACh-induced AHP changes and ACh intensities that generally concur with this experimental data, shown in Table 4 and Table 5, respectively. By combining these estimates, we arrive at five intensities of ACh modulation, labeled "Low", "Basal", "Moderate", "High" and "Very High", with corresponding states of different AHP conductances, depicted in Table 6. Simulations were performed at these five intensities.

Table 6 Model AHP conductances for cholinergic intensities

ACh			AHP Conductances (% of Basal)		
Intensity	% of Basal	Conc (µM)	g_{fAHP}	g_{mAHP}	g_{sAHP}
Low	50	0.25	75	110	135
Basal	100	0.50	100	100	100
Moderate	150	0.75	125	90	65
High	200	1.00	150	80	30
Very High	250	1.25	175	70	0[g]

[g]We assume that AHPs do not invert into ADPs

2.6 Spiking stimulation and synaptic models

For stimulation, an input spike train is used to replicate *in vivo* signaling. In particular, EPSPs recorded in single cells exhibit a long tailed distribution of peak amplitudes and show increased reliability of synaptic transmission with increasing amplitude (Markram et al. 1997; Song et al. 2005). In other words, the excitatory synaptic inputs to a single cell consist of several strong driving synapses amongst a sea of weak synapses. Because of this diversity of synaptic strength, we evaluate the strong connection case as *homosynaptic* stimulation, in which a spike train arrives at a single synapse. In this homosynaptic case, the connection strength is strong, the input frequency range is low (~100 spikes/sec), and the synaptic model should ideally account for limited postsynaptic receptors and neurotransmitter saturation:

$$I_{AMPA} = g_{AMPA} g_{SD}(t, \tau_{r,AMPA}, \tau_{f,AMPA}, H_I)(E_{AMPA} - V_d), \tag{40}$$

where g_{AMPA} = 2.5pS and g_{SD} is the *saturating differentials* waveform.

In contrast, we evaluate the weak connection case as *heterosynaptic* stimulation, in which a spike train converges on the cell across numerous independent synapses. In this heterosynaptic case, the connection strengths are weak, the input frequency range is high (~1000 spikes/sec), and the synaptic model treats EPSPs independently; i.e., without a saturation restriction.

$$I_{AMPA} = g_{AMPA} g_{IE}(t, \tau_{r,AMPA}, \tau_{f,AMPA}, H_I)(E_{AMPA} - V_d), \tag{41}$$

where g_{AMPA} = 0.1pS and g_{IE} is the *independent exponentials* waveform. This approach relies on the assumption that spikes from non-driving inputs arrive at most individual synapses at a low enough rate (e.g., less than 80 spikes/s) and hence saturation complexities are negligible. Indeed, average firing rate in cortex varies by cell type, region, and layer, but excitatory cells normally stay within a low firing range. For example, pyramidal neuronal firing in cortical area V4 in rhesus macaque varies between about 4 Hz and 16 Hz depending, on whether preferred Gabor stimuli entered the cell receptive field (Mitchell et al. 2007). We employ both cases to evaluate the impact of different forms of input signaling.

With all synaptic models, the rise and fall rates of EPSPs remain identical and their parameters are derived from recordings of currents from pyramidal cells of rat prefrontal cortex

layer 2/3 (Povysheva et al. 2006). The parameters for the AMPA current are E_{AMPA} = 0mV, and time constants $\tau_{r,AMPA}$ = 0.76 ms and $\tau_{f,AMPA}$ = 6.5 ms, which fall in a range similar to other cortical experimental data; e.g., $\tau_{r,AMPA}$ = 0.9 ms and $\tau_{f,AMPA}$ = 3.1 ms for current through AMPA receptors in neocortical layer 4 pyramidal and interneuron cells of the rat visual cortex (Watt et al. 2000) and $\tau_{r,AMPA}$ = 0.3 ms, $\tau_{f,AMPA}$ = 2.2 ms for layer 1 neurons in rat visual cortex (Hestrin and Armstrong 1996). We analyze both the heterosynaptic and homosynaptic cases to evaluate whether the results hold for both a signal input source (a single presynaptic cell) and multiple convergent sources (multiple presynaptic cells).

2.7. Mapping between parametric and operational space

A major target of this study is to examine the relation that is mediated by the signal function between the parametric space of a cell's biophysical properties and the operational space of its transformational properties. Because we are concerned with evaluated the AHP currents, we distill the parametric space into the strength of these currents. The parametric space is then a non-negative vector space, denoted G, that consists of three-dimensional vectors of the AHP peak conductances:

$$\vec{g} = \begin{bmatrix} g_1 \\ g_2 \\ g_3 \end{bmatrix} = \begin{bmatrix} g_{fAHP} \\ g_{mAHP} \\ g_{sAHP} \end{bmatrix}. \tag{42}$$

For example, with this notation, the basal level of AHP conductances can be denoted as:

$$\vec{g}_0 = \begin{bmatrix} 0.80\,pS \\ 0.04\,pS \\ 0.02\,pS \end{bmatrix}. \tag{43}$$

The operational space is also treated as a non-negative vector space, denoted Z, of three-dimensional vectors whose entries characterize sigmoid signal shape; namely:

$$\vec{z} = \begin{bmatrix} z_1 \\ z_2 \\ z_3 \end{bmatrix} = \begin{bmatrix} t \\ s \\ y_M \end{bmatrix}, \tag{44}$$

$t, s,$ and y_M denote the sigmoid threshold, slope and upper asymptote, respectively. For each vector of parameters, we ran simulations for 2000 simulated milliseconds in duration, each stimulated by a regular spike train at a specific input rate, and observed the average output spike rate. Each input and output firing rate pair from each simulation provided a data point in the transfer function. The cell's transfer function was then fit by minimizing the root mean square error to the four-parameter function:

$$Q(y) = y_0 + \frac{(y_M - y_0)}{1 + e^{-4s(y-t)/(y_M - y_0)}}, \tag{45}$$

where y_0, y_M, t, and s corresponds to lower asymptote, upper asymptote, threshold, and slope, respectively. The lower asymptote is excluded from operational space, because lower asymptote was not significantly affected by changes in AHP conductances. Nonetheless, it is necessary to include it in Eq. (45) in order to obtain good fits of the sigmoid functions.

Having established both a parametric space of a cell's biophysical properties and an operational space of its signaling, we can define for this cell model a mapping f between the parametric space G and the operational space Z:

$$f : G \rightarrow Z . \tag{46}$$

The mapping f determines how changes in membrane conductances map to the cell's signaling. As an example, if we apply the mapping f to the vector of basal levels of AHP conductances, g_0, from Eq. (43), this yields the main features of our transfer function in the vector z_0:

$$f(\vec{g}_0) = \vec{z}_0 . \tag{47}$$

This definition provides a formalism to define the properties of this mapping f, such as whether the conductance parameters control the transfer function shape in a linear way.

All simulations were performed in MATLAB Simulink with a 0.02ms maximum variable step size using Dormand-Prince integration on dual Intel Xeon quad-core processors (8 CPUs) in a Windows XP x64 environment.

3   Results

3.1 Spike-dependent signals

An individual excitatory postsynaptic potential (EPSP) occurs as a time-varying conductance wave after each arriving presynaptic (or input) spike, while an after-hyperpolarization (AHP) current results from a time-varying conductance wave after each postsynaptic (or output) spike. Because both the input signal and the AHP currents are crucial aspects of the cell transfer function and can be considered spike-dependent signals, we begin with an analysis of three forms of the signals, described in Section 2.2. The three forms of spike-dependent signals (*independent exponentials*, *normalized exponentials*, and *saturating differentials*) were first compared in isolation by evaluating Eq. (14), (15), and (17) respectively with $\tau_r = 1$ ms and $\tau_f = 10$ ms. For all the models, a single spike generates nearly identical waveforms (Fig. 2a, b). The *saturating differentials* form has a slightly slower rise time, while the *independent exponentials* form has a slightly faster fall time. Given that the signals are driven by a spike train with an interspike interval of 10ms (i.e., a regular stimulation rate of 100 spikes/sec), the second spike causes a distinguishably different waveform for each spike- dependent model (t=20-30ms in Fig. 2bc). With the *normalized exponentials* model, the conductance peaks at the same amplitude as it did during the first peak, while with the other two models, the second peak exceeds the first as a result of temporal summation.

Evaluation over 2000 ms quantifies the effect further. Here, the maximal conductance as a proportion of the peak conductance following a single spike again distinguishes the models. While conductance remains static for the *normalized exponentials* model, the maximal conductance increases with the input rate, especially beyond 50 spikes/sec, for both the *independent exponentials* and the *saturating differentials* models (Fig. 2 b,c). In a low 0-100 spikes/s range, these two models increase similarly (Fig. 2c). In the high 0-1000 spikes/s range, conductance for the *independent exponentials* model increases approximately linearly with rate, whereas for the *saturating differentials* model, the maximal conductance saturates (Fig. 2d). If the signal is slowed by an order of magnitude by setting $\tau_r = 10$ ms and $\tau_f = 100$ ms, temporal summation begins at lower frequencies (Fig. 2e). The temporal summation causes the *independent exponentials* form to exhibit a greater slope in maximal conductance. The maximal conductance for the *normalized exponentials* form declines at high spike rates. Because Eq. (15) only accounts for the last two spikes, new spikes terminate the rise in conductance from previous

spikes. The *saturating differential*s form asymptotes to the same conductance as with the faster time constants.

The results of the analysis of spike-dependent signals was used to select which of the three forms to use for both input signals and AHP currents in the subsequent cell simulations. Since the *saturating differential*s form approaches a saturation level given a prolonged high firing rate, yet does not decline at very high firing rates as the *normalized exponentials* form does, we selected the *saturating differential*s form for the spike-modulated AHP currents to portray the saturation of a limited channel resource. These equations are detailed in Sections 2.3.

For synaptic input, the saturation of channel capacity depends on whether the input arrives at an individual synapse, namely *homosynaptically*, or at multiple independent synapses, namely *heterosynaptically*. The *saturating differential*s form was chosen for the homosynaptic case, since we expect synaptic saturation. The *normalized exponentials* form was chosen for the heterosynaptic case, since we do not expect synaptic saturation if spikes arrive from independent non-bursting source cells. This is further detailed with equations in Sections 2.6.

3.2 Spike-based vs calcium-based AHP

For both the *spike-based* and *calcium-based* AHP cell models, conductances and other parameters for each AHP current were adjusted until peak amplitudes (mV), rise time, and fall time constants were comparable to physiological measurements (see Section 2.4 and Table 3). The *calcium-based* model depicted in Fig. 3e was also tuned to have similar temporal profiles to the *spike-based* model for all three AHP currents (Fig. 3c, d). Notably, the mAHP and sAHP current in the *calcium-based* model use the same SK channel activation and inactivation, and their time courses are distinguished by the calcium source on which they depend.
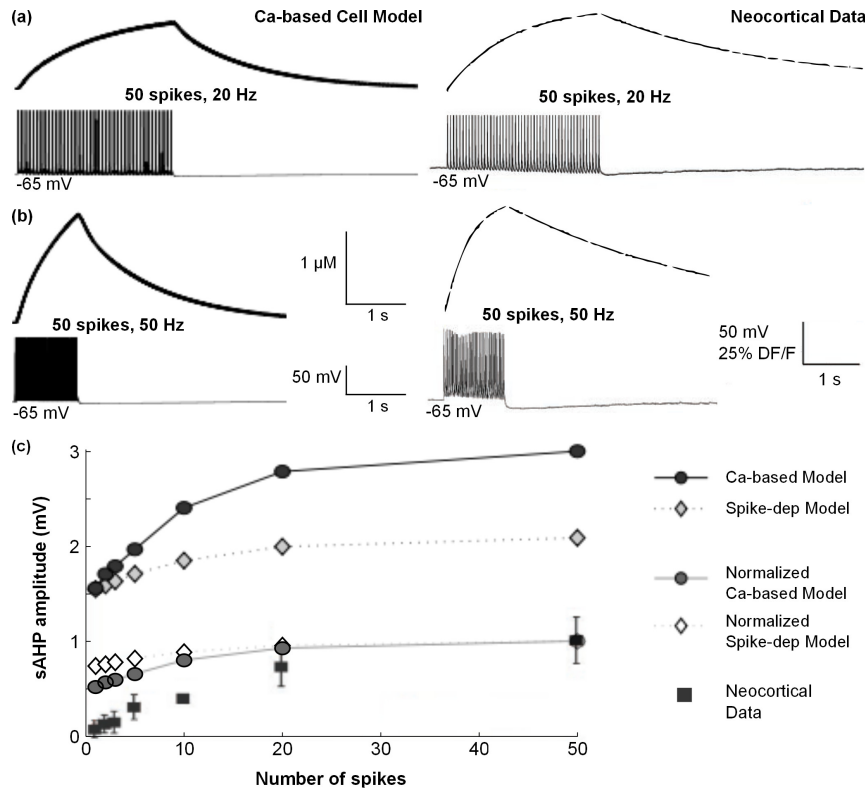

Fig. 4 Calcium accumulation and rise in sAHP.
(**a,b**) Accumulation of calcium in the *calcium-based* cell model (leftside) compared with pyramidal layer 2/3 cells from rat neocortex (rightside; Abel et al. 2004) during 50 spikes at (**a**) 20 spikes/sec and (**b**) 50 spikes/sec.
(**c**) Consequent rise in sAHP depending on the number of induced spikes at 50 spikes/sec for both the *spike-based* and *calcium-based* cell model compared with sAHP measurements from the same neocortical data

24

We compared the calcium accumulation and the consequent rise in sAHP conductance for the *calcium-based* cell model with data from pyramidal layer 2/3 cells of rat neocortex (Abel et al. 2004). Accumulation of somatic calcium, evaluated as the sum of $[Ca_C]$ and $[Ca_S]$ in the *calcium-based* cell model, over the course of 50 stimulation spikes at either 20 spikes/sec and 50 spikes/sec had a escalating profile that is comparable with neocortical data, albeit with a slighter faster decay (Fig. 4a, b). Since sAHP is dependent on this calcium accumulation, we expect to observe a consequent rise in sAHP amplitude. The sAHP amplitude (measured as voltage in mV for a cell with sAHP subtracted from a cell without sAHP) does rise depending on the number of induced spikes at 50 spikes/sec for both the *spike-based* and *calcium-based* cell model (Fig. 4c). Both models exhibit a higher sAHP amplitude compared with measurements from neocortical data (Abel et al. 2004). Nonetheless, the profiles are qualitatively similar. After normalization, the curvature for the *calcium-based* cell model is closer to the data than that for the *spike-based* model.
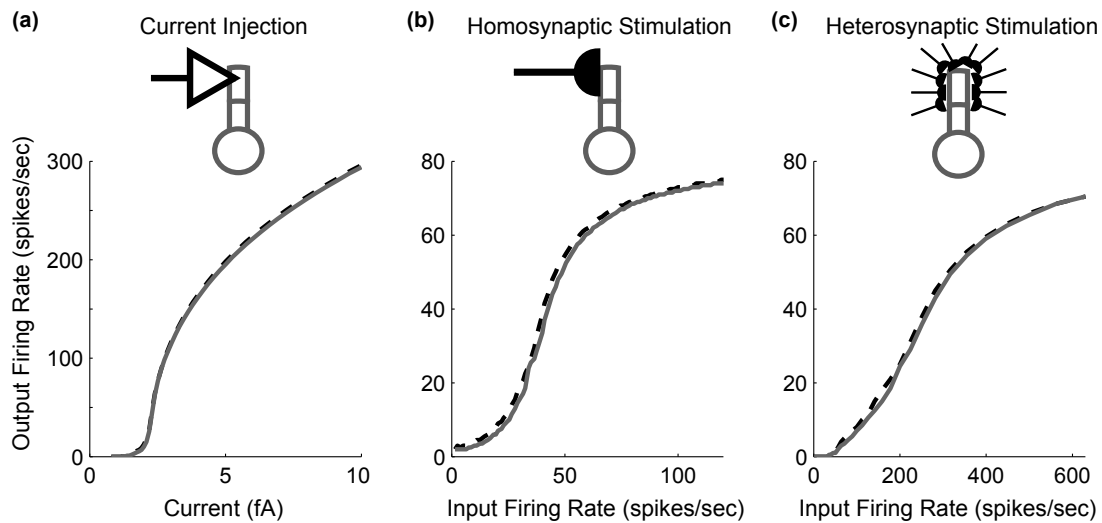

Fig. 5 Sigmoid transfer function and stimulation comparison. (**a**) Output firing rate as a function of the current injection into the distal dendrite. (**b**) Transfer functions of both spiking models with basal physiological levels of fAHP, mAHP and sAHP currents. Stimulated in the low range (0-100 spikes/s) with strong (2.5 pS) AMPA conductance and *saturating differentials* synapses (homosynaptically), and (**c**) in the high range (0-1000 spikes/s) with weak (0.1 pS) AMPA conductance and *independent exponentials* synapses (heterosynaptically). (**a-c**) Solid line denotes the *spike-based* AHP model and dashed line denote the *calcium-based* AHP model

3.3 Sigmoid transfer function and stimulation comparison

To test the responsiveness of the cell models, we stimulated both with an current injected into the distal dendrite (Fig. 5a), and evaluated the transfer function of the cell with basal physiological levels of fAHP, mAHP and sAHP currents. Simulations led to transfer functions of an asymmetric sigmoidal form. The spiking models were stimulated homosynaptically, that is with *saturating differentials* synapses and with strong (2.5 pS) peak AMPA conductance over a low input range (0-100 spikes/s). This stimulation protocol generates a sigmoidal transfer function with as input threshold of 32 spikes/s and output asymptote of 80 spikes/s (see Fig. 5b). The

spiking models were also stimulated heterosynaptically, that is with *independent exponentials* synapses and with weak (0.1 pS) peak AMPA conductance over a high input range (0-1000 spikes/s). This generates sigmoidal transfer functions with an input threshold of 220 spikes/s and an output asymptote of 75 spikes/s (Fig. 5c). Excitability across these conditions is similar for the s*pike-based* AHP model (solid line) and for the *calcium-based* AHP model (dashed line).
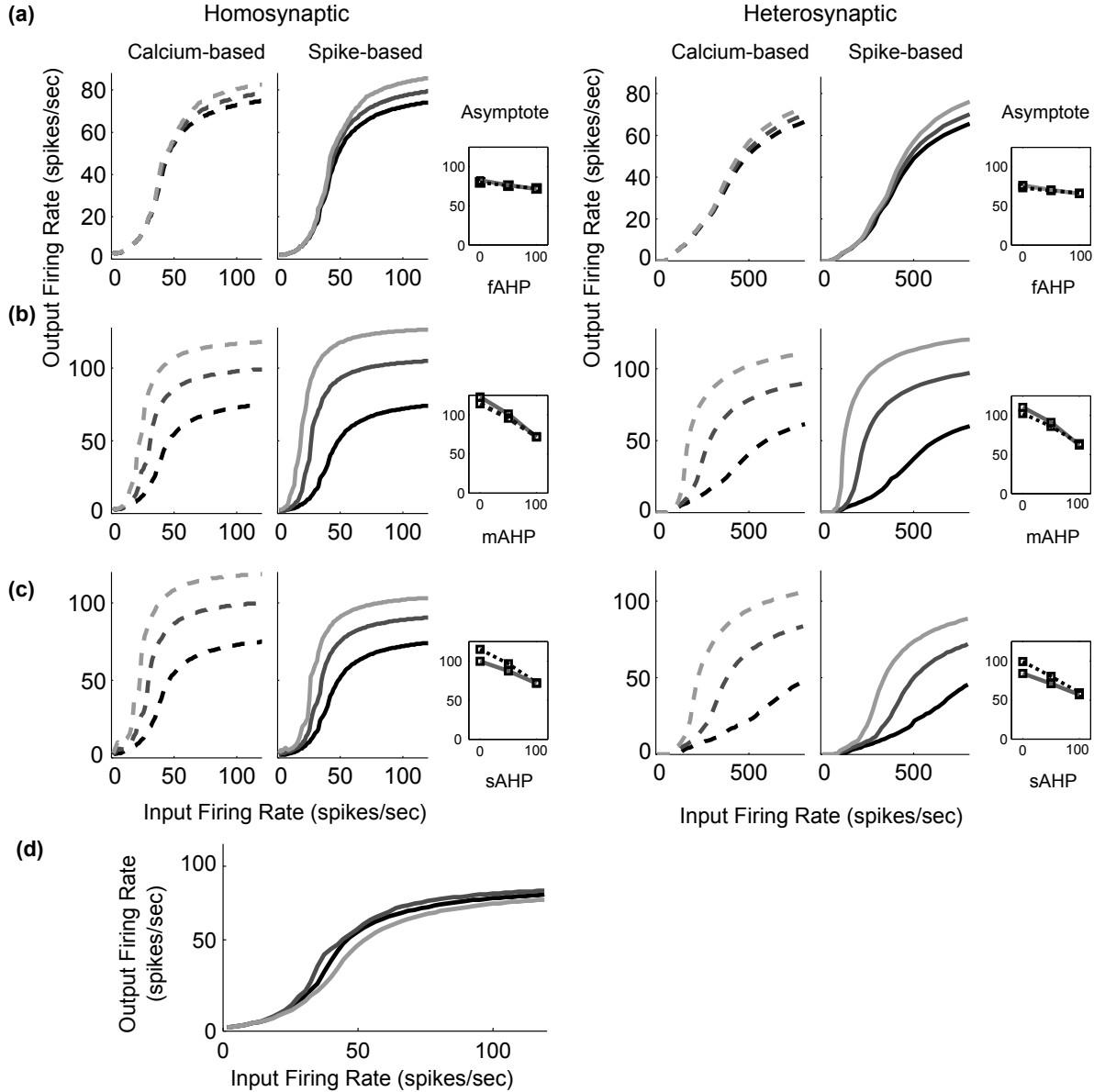
Fig. 6 Contribution of individual AHP currents to transfer function. Spiking model stimulated homosynaptically (left two columns) and heterosynaptically (right two columns), as Fig. 5b and 5c respectively with (**a**) diminishing fAHP currents, (**b**) diminishing mAHP currents and (**c**) diminishing sAHP currents. Inlaid plots show the change in asymptote of transfer function, measured by sigmoidal curve fits, as a function of conductance change for each AHP current. Solid line denotes the *spike-based* AHP model and dashed line denote the *calcium-based* AHP model. (**d**) Conservation of output asymptote with changes to AHP currents limited to two different pairs, fAHP and mAHP. This example uses the *calcium-based* model

3.4 Individual AHP effects and asymptote conservation

All AHP currents tested affect the asymptote, or maximum value, of the sigmoid signal function. Reduction of the fAHP current raises the asymptote, thereby also causing an increased slope (Fig. 6a). Reduction of the mAHP current reduces the region near the point of inflection or threshold more than the other two currents, but does so while simultaneously increasing the slope and asymptote (Fig. 6b). Finally, reduction of the sAHP current affects mainly the lower range of the transfer function where the output firing rate is low, decreasing threshold and slope (Fig. 6c). To quantify the changes in the asymptote, we evaluate the variable y_M in Eq. (27), which is the asymptote resulting from a regression fit of the transfer functions in Fig. 6a-c. We observe how this value changes, Δy_M, with respect to changes in the conductances of the fAHP current, Δg_{fAHP}, the mAHP current, Δg_{mAHP} and the sAHP current, Δg_{sAHP}. The values of y_M as a function of g_{fAHP}, while g_{mAHP} and g_{sAHP} remain constant, can be fit with a linear regression:

$$y_M = A_f g_{fAHP} + B_f . \tag{48}$$

Likewise, we can fit y_M as a function of g_{mAHP} and g_{sAHP}:

$$y_M = A_m g_{mAHP} + B_m \tag{49}$$

and

$$y_M = A_s g_{sAHP} + B_s . \tag{50}$$

With the simulations depicted in Fig. 6, we compute that $A_f = -11$, $A_m = -51$, $A_s = -28$ for the spike-based AHP model and $A_f = -7.7$, $A_m = -41$, $A_s = -43$ for the calcium-based AHP model. The derivatives of Eq. (48)-(50) produce estimates of how changes in AHP conductances will effect the asymptote:

$$\Delta y_M = A_f \Delta g_{fAHP}, \tag{51}$$

$$\Delta y_M = A_m \Delta g_{mAHP}, \tag{52}$$

and

$$\Delta y_M = A_s \Delta g_{sAHP}. \tag{53}$$

Since we expect these changes to act roughly independently within a close range around the basal state, Eq. (51)-(53) can then be combined into a generalized form:

$$\Delta y_M = A_f \Delta g_{fAHP} + A_m \Delta g_{mAHP} + A_s \Delta g_{sAHP}. \tag{54}$$

AHP conversation law. The intrinsic properties of the cell are known to change in a homeostatic way to maintain the output firing range (Turrigiano et al. 1994), and recent data suggest that AHP currents might play a role in this homeostasis of output rate (Karmarkar and Buonomano 2006; Santini et al. 2008). Therefore, we ask whether the output asymptote could be conserved as the three AHP currents change collectively. With the relation expressed by Eq. (54), we can immediately conjecture what parametric manipulations of the conductances will conserve the asymptote of the output firing rate. By setting $\Delta y_M = 0$, this yields a *conservation law* for this property; namely:

$$A_f \Delta g_{fAHP} + A_m \Delta g_{mAHP} + A_s \Delta g_{sAHP} = 0 \tag{55}$$

implies that the asymptote does not change. If this equation holds for small changes in AHP, then it represents a local linearity (and a local homomorphism) between parametric changes and the operational space of constant y_m. Since, all the coefficients, evaluated numerically, have the same sign, this establishes a balancing act. For example, when one AHP conductances rises, another one must decrease if the output asymptote of the cell is to be the same firing rate. Formally, we

can break Eq. (55) into sub-equations by considering the conductances in pairs, and setting Δg_{fAHP}, Δg_{mAHP}, or Δg_{sAHP} each to zero:

$$\Delta g_{fAHP} = (A_m / A_f)\Delta g_{mAHP}, \tag{56}$$

$$\Delta g_{fAHP} = (A_s / A_f)\Delta g_{sAHP}, \tag{57}$$

and

$$\Delta g_{sAHP} = (A_m / A_s)\Delta g_{mAHP}. \tag{58}$$

Eq. (52)-(54) can then be used individually or in combination to maintain the asymptote. For instance, if the mAHP conductance increased, then the sAHP conductance could decrease in ratio governed by Eq. (58), while the fAHP conductance remained the same. Fig. 6d confirms this analysis by showing that changes in pairs governed by Eq. (56)-(58) maintain the asymptote in the three plots, respectively.

3.5 Threshold and slope transformations

Next, we assess the capability of AHP currents to control transfer functions. The analysis is done independently from Acetylcholine or other neuromodulatory signals, but is partly meant to capture the potential of such modulatory signals. To do this, we search for parametric transformations on the 3 AHP conductances which affect a single dimension in the operational space, either the threshold or slope of the transfer function of the basal cell. In other words, we are looking for a set of changes in AHP magnitudes that shifts the threshold of the transfer function without significantly altering the slope or the asymptote (and vice versa for slope). Unlike with the asymptote of the output, we are not concerned with conservation or homeostasis, but rather with the ability of the AHP currents to control the other two main degrees of freedom of transfer function shape independently. As previously discussed, we expect these two degrees of freedom to be pivotal in determining both the quenching threshold and contrast enhancement in a cortical network, based on the work of Grossberg and colleagues (Grossberg 1973, 1980; Grossberg and Levine 1975). These two primary operations for the sigmoid shape, we will abstractly call T and S which shift the threshold and increase slope respectively. Formally, we seek to demonstrate, at least within a local range, that there exists a corresponding parametric transformation T_g that consistently maps (via our functional mapping f from Eq. (46)) to a threshold shift T_z and determine whether the transformation across the mapping scales linearly by scaling factor A:

$$f \circ AT_g = AT_z \circ f, \tag{59}$$

where $\circ$ denotes the function composition, that is the application of one function to the results of another, $(h \circ f)(\bar{g}) = h(f(\bar{g}))$ for all $\bar{g}$ in G. Conceptually, the mapping f captures how changes in membrane conductances (or parametric space G) map to cell signaling (operational space Z). Applying the mapping f to a vector of AHP conductances, g, from Eq. (42), this yields the main features of our transfer function in the vector z:

$$f(\bar{g}) = \bar{z}. \tag{60}$$

T_z in operational space is expressed as:

$$T_z : \bar{z} \to \bar{z}' \text{ such that } \begin{bmatrix} z_1' \\ z_2' \\ z_3' \end{bmatrix} = \begin{bmatrix} z_1 \\ z_2 \\ z_3 \end{bmatrix} + \begin{bmatrix} T_{\Delta z} \\ 0 \\ 0 \end{bmatrix}. \tag{61}$$

Similarly, we seek to demonstrate, again within a local range, that there exists a parametric transformation S_g that consistently maps (via the function mapping f) to a slope change S_z by a scaling factor B:

$$f \circ BS_g = BS_z \circ f , \tag{62}$$

where S_z in operational space is expressed:

$$S_z : \vec{z} \to \vec{z}' \text{ such that } \begin{bmatrix} z_1' \\ z_2' \\ z_3' \end{bmatrix} = \begin{bmatrix} z_1 \\ z_2 \\ z_3 \end{bmatrix} + \begin{bmatrix} 0 \\ S_{\Delta z} \\ 0 \end{bmatrix}. \tag{63}$$

In so doing, we assume that purely translational affine transformations, fairly basic operations, will act as sufficient parametric transformations to roughly satisfy (60)-(63), and denote them:

$$T_g : \vec{g} \to \vec{g}' \text{ such that } \begin{bmatrix} g_1' \\ g_2' \\ g_3' \end{bmatrix} = \begin{bmatrix} g_1 \\ g_2 \\ g_3 \end{bmatrix} + \begin{bmatrix} T_{g1} \\ T_{g2} \\ T_{g3} \end{bmatrix}, \tag{64}$$

and

$$S_g : \vec{g} \to \vec{g}' \text{ such that } \begin{bmatrix} g_1' \\ g_2' \\ g_3' \end{bmatrix} = \begin{bmatrix} g_1 \\ g_2 \\ g_3 \end{bmatrix} + \begin{bmatrix} S_{g1} \\ S_{g2} \\ S_{g3} \end{bmatrix}. \tag{65}$$

We find an operation T_g for a rightward shift in the threshold of the transfer function for the *spike-based* AHP model to be (Fig. 7a):

$$\begin{bmatrix} T_{g1} \\ T_{g2} \\ T_{g3} \end{bmatrix} = \begin{bmatrix} -0.360\,\text{pS} \\ 0.0020\,\text{pS} \\ 0.0003\,\text{pS} \end{bmatrix}. \tag{66}$$

Applying this operation two times (A=2 for Eq. (59), such that fAHP, mAHP and sAHP were 10%, 110% and 103% of basal conductance respectively), the sigmoid threshold shifts to 114% of basal level (slope to 81%, asymptote to 99%). For an increase in the slope of the transfer function for the *spike-based* AHP model, we find an operation S_g to be (Fig. 7b):

$$\begin{bmatrix} S_{g1} \\ S_{g2} \\ S_{g3} \end{bmatrix} = \begin{bmatrix} 0.004\,\text{pS} \\ -0.008\,\text{pS} \\ 0.008\,\text{pS} \end{bmatrix}. \tag{67}$$

Applying this operation two times (B=2 for Eq. (62), such that fAHP, mAHP and sAHP were 101%, 60% and 180% of basal conductance respectively), the sigmoid slope steepens to 127% of basal level (threshold to 85.9%, asymptote to 101%).

Ideally, the two operations T and S would act as operators that exhibit three properties: linearity, independence and orthogonality. Linearity implies that the effect of the operations scale such that:

$$f \circ T_g = T_z \circ f \to f \circ AT_g = AT_z \circ f \tag{68}$$

and

$$f \circ S_g = S_z \circ f \to f \circ BS_g = BS_z \circ f . \tag{69}$$

Testing integer values of A and B (i.e. repetition of operators) produces an upward curvature in threshold and slope, (central inlaid plots in Fig. 7a, b), indicating that the operators do not scale linearly.
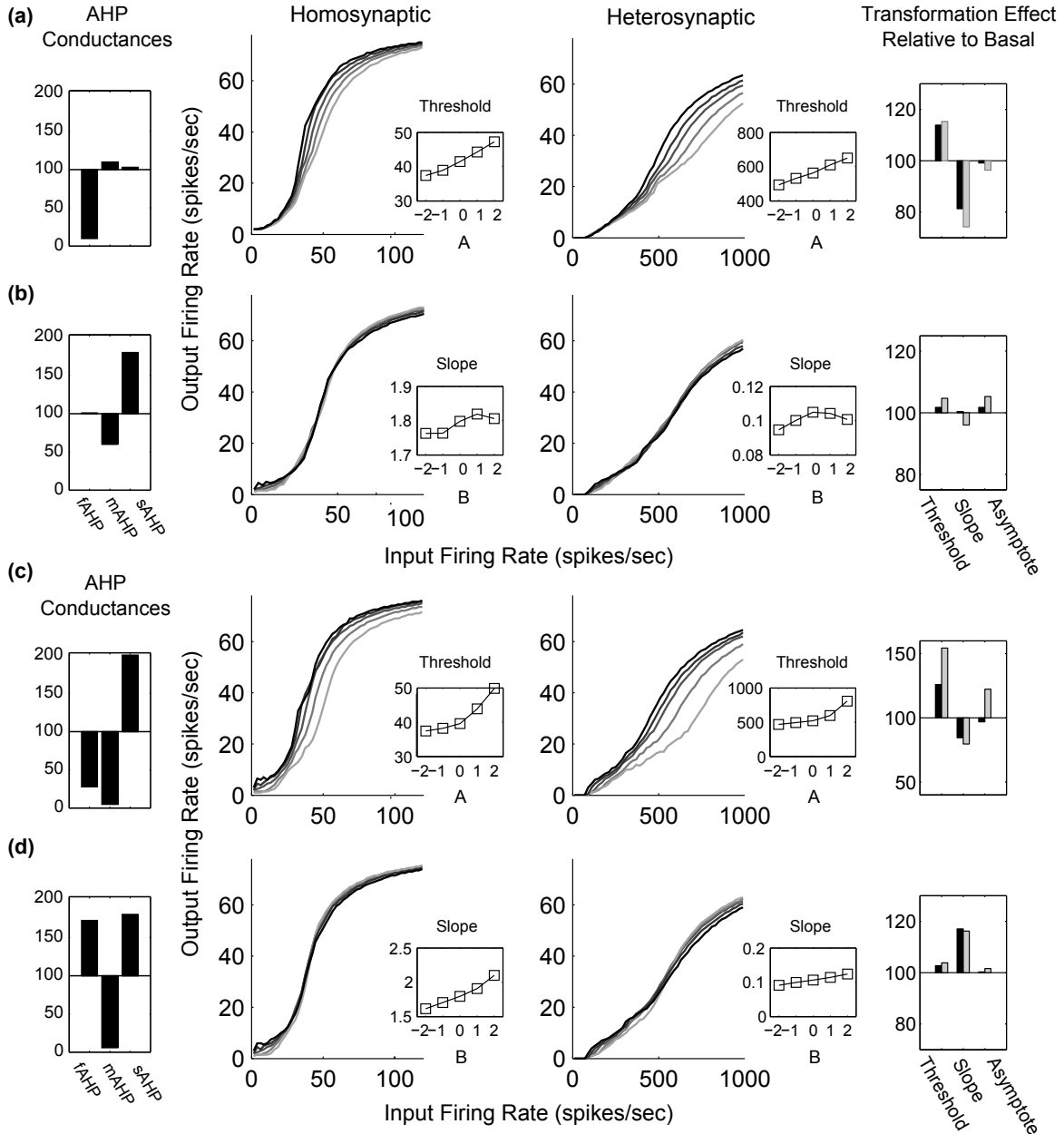
Fig. 7 Threshold and Slope Change. Transfer function of the *spiked-based AHP* cell (**a**) under variation in threshold translation and (**b**) under variation in slope, shown for homosynaptic stimulation (left middle column) and heterosynaptic stimulation (right middle column). Inlaid plots depict the threshold/slope as measured by fit as a function of the parametric operation magnitude (A or B from Eq. (59) and (62)). The right column quantifies how pure the operations are in their respective dimensions with black corresponding to homosynaptic stimulation and grey corresponding to heterosynaptic stimulation. (**c, d**) The same as (a,b) instead with the *spiked-based AHP* cell

3.6 Cholinergic modulation

We then evaluate the impact of cholinergic modulation on the cell's transfer function. Here, varying levels in Acetylcholine cause fluctuations in the AHP currents, which in turn affect the transfer functions. Simulations were performed at these 5 intensities, "Low", "Basal", "Moderate", "High" and "Very High", (shown in Table 6), which correspond to relative behavioral ACh concentrations (detailed in Table 5). Increased ACh causes a leftward threshold shift under both synaptic stimulation approaches (81%, 66%, and 58% of basal threshold for "Moderate", "High", and "Very High" ACh, respectively, with the *spike-based AHP* model, and 79%, 64%, and 55% with the *calcium-based AHP* model). There was also a change in slope, which depending on the synaptic stimulation (227% for *spike-based*, 252% for *calcium-based* models under "Very High" ACh) and an increase in the asymptote of the transfer function (147% for *spike-based*, 164% for *calcium-based* models under "Very High" ACh). The reverse effect of increased threshold occurs with "Low" ACh intensity (125%, 41%, 70% of basal threshold, slope, and asymptote, respectively, for the *spike-based AHP* cell). Fig. 8 depicts the full results for ACh intensities.

We note that, because all three AHP conductances change in the same direction for cholinergic modulation as for the abstracted threshold translation operator T_g, both manipulations produce a similar shift. However, since the relative proportions differ, the effect of ACh modulation is not purely threshold translation.

4 Discussion

4.1 AHP effects on sigmoid signalling

The work presented here incorporates a broad set of observed AHP currents of differing timescales to demonstrate how the collective state of the AHP conductances can control the shape of sigmoidal signal functions by translating its threshold and changing its slope independently and orthogonally. The specific conditions for a leftward threshold shift were established to occur when the sAHP and mAHP currents decrease, while fAHP current increases, at the appropriate ratios. Likewise, we determine the conditions, under which the slope of the transfer function becomes steeper, to be when the sAHP and fAHP currents decrease, while mAHP current increases, at the appropriate ratios. The analysis defines threshold and slope manipulations as operations, which occur in the parametric space of cell membrane conductances, and can be mapped onto the operational space of cell signaling, described by threshold, slope and asymptote. Applying these operations in combination in the parametric space, we observe the effect after the mapping into the operational space to behave roughly orthogonally within a range around basal conditions.

The computational model presented herein further quantifies the effects on cholinergic modulation on the shape of the transfer function. Simulation of cholinergic modulation over the full array of physiologically observed AHP currents predominantly cause a translation of the threshold in cell sigmoidal transfer function alongside an asymptote and slope change rather than just a gain in cell excitability. This provides additional detail beyond the traditional description, which lumps distinct AHP currents together, shown in other models to cause an increased gain on sensory input (Giocomo and Hasselmo 2007; Sarter et al. 2005). The aforementioned model of pyramidal cells from piriform cortex (Barkai and Hasselmo 1994), for example, represents ACh modulation as a decrease in a single AHP current and an m-current. Similarly, a model of cells in primary visual cortex by Wang and colleagues does include both a Na^+-dependent K^+ current and a Ca^{2+}-dependent K^+ current to explain adaptation on two different timescales (Wang

et al. 2003). In summary though, these models do not account for the full set of observed AHP currents, nor do they quantify the relative changes in threshold, slope and asymptote of signaling under different cholinergic stimulation intensities.
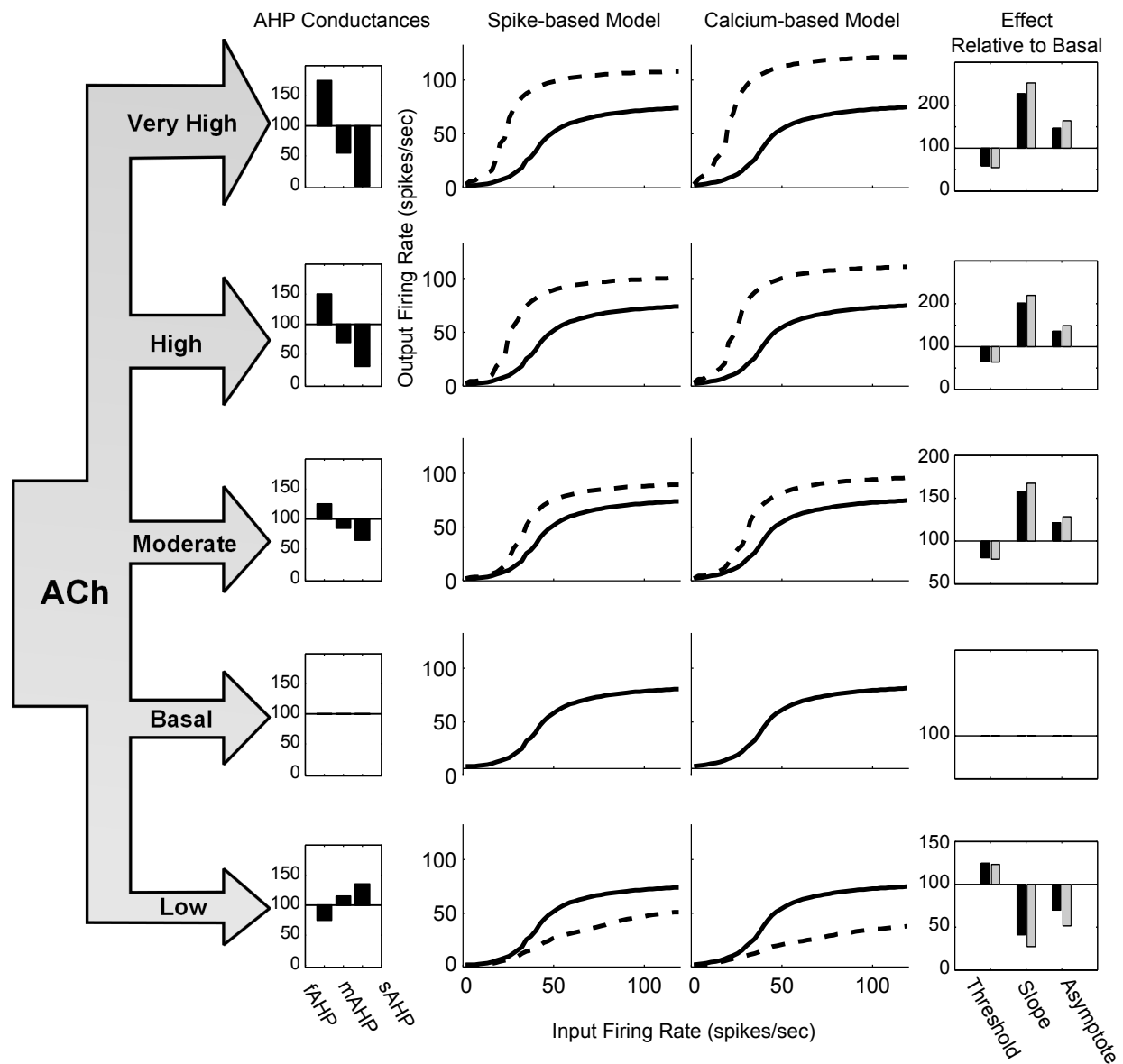
Fig. 8 Impact of cholinergic intensity on AHP and cell transfer function. As ACh increases over 5 intensities ("Low", "Basal", "Moderate", "High" "Very High"), AHP conductances (left column) vary in proportion, and transfer function shifts leftward for both homosynaptic stimulation (left middle column) and heterosynaptic stimulation (right middle column). These effects are quantified in operational space (right column) with black and gray corresponding to homosynaptic and heterosynaptic stimulation respectively

The results show how *parametric space* of cell membrane conductances can be mapped onto the *operational space* of cell signaling, as described by threshold, slope and asymptote of the transfer function. Understanding how membrane properties affect the dynamics of individual

cells is a chief concern for both neural modelers and neurophysiologists. Several studies have tackled the problem of describing how biophysical cell parameters determine functional behaviors of spiking neuron models. For instance, Prinz et al. (2003) characterized steady state behavior of compartment models as either silent, tonically active, bursting, or non-periodic when cell membrane conductances were varied over 6^8 permutations. In this and related work on exploring the parametric space of spiking neurons (Taylor et al. 2006; Van Geit et al. 2007; Weaver and Wearne 2008), model neurons were stimulated with injection currents or holding voltages to emulate physiological techniques like electrode stimulation and voltage clamp. However, this approach often fails to accurately portray the character of inputs that a cell may receive *in vivo*, and it obscures potential signaling mechanisms by warping temporal integration and by damping oscillatory, rebound, and reverberant behaviors. We build upon these ground breaking analyses by considering more realistic synaptic models.

4.2 Vigilance control, hypothesis testing, and learned generalization
It is crucial to understand not only which internal cell dynamics determine the transfer function, but also how these dynamics may be regulated by the larger system. This is noted especially in memory systems, such as those described by Adaptive Resonance Theory, or ART (Bullier et al. 1988; Carpenter and Grossberg 1987, 1991; Engel et al. 2001; Fries et al. 2001; Gao and Suga 1998; Grossberg 1998, 1999, 2003; Krupa et al. 1999; Pollen 1999; Sillito et al. 19994; Ursey 2002). Findings about the behavioral and pharmacological dynamics of ACh (Descarries and Umbriaco 1995; Hsieh et al. 2000) and its neuromodulatory effect on AHP currents (Giocomo and Hasselmo 2007; McCormick and Williamson 1989; Vogalis et al. 2003) provide evidence for how modulatory signals could control cortical transfer functions for mode shifts in cortical network dynamics. Indeed, the major cortical effect of cholinergic innervations is considered to be the reduction of after-hyperpolarization (AHP) currents, which results in the increase of cell excitability (Saar et al., 2001). In an ART system, augmented cortical excitability due to predictive mismatch may cause reset of currently active cognitive recognition codes, or categories, even in cases where top-down feedback may earlier have partially matched bottom-up input. As noted in Section 1.3, this increase of excitability is mediated by the gain, called *vigilance*, of the process whereby bottom-up input patterns are matched against learned top-down expectations.

　　Grossberg and Versace (2008) proposed that the release of ACh might increase vigilance and thereby promote search for finer recognition categories in response to mismatch-inducing environmental feedback. In a similar manner, vigilance might increase in response to a release of ACh in response to stress factors such as shock (Zhang et al. 2004), even when bottom-up and top-down signals have a good match based on similarity alone. Anatomical studies in monkeys, cats and rats have established that the nonspecific thalamus (in particular, the midline and central lateral thalamic nuclei), whose activation is sensitive to the degree of mismatch between cortical expectations and sensory stimuli (Kraus et al. 1994), projects to the cholinergic nucleus basalis of Meynert (van Der Werf et al. 2002), one of the main sources of cholinergic innervations of the cerebral cortex. The terminals of cholinergic pathways, as revealed by choline acetyltransferase immunostaining, exhibit a low synaptic incidence of about 14% in cortex (Descarries and Umbriaco 1995; Mechawar et al. 2002; Umbriaco et al. 1994). These terminals flood the extracellular space with ACh diffusely and provide a global signal to widely distributed cells.

　　Our analysis treats AHP changes as operations on cellular signal transformation to better characterize the resulting cell behavior and the impact of increased/decreased ACh on network

dynamics and learning. The results are in agreement with other simulation and theoretical work suggesting that ACh may act as a vigilance signal. In ART systems, bottom-up processing is modulated by top-down learned expectations that embody predictions or hypotheses that focus attention on expected bottom-up stimuli. If the top-down expectation is a close enough match to the bottom-up input pattern, the network locks into a resonant state through a positive feedback loop that dynamically links, or binds, the attended features with their category via top-down attentional signals. Within this resonant state, the network undergoes a refinement of the expected categorical representation with the current features during the learning episode. This *match-based learning* process is the foundation of the stability of learned cognitive codes in an ART model. Match-based learning allows memories to change only when the input from the external world is close enough to internal expectations, or when something completely new occurs. In this way, top-down attention carries out a form of "biased competition" (Desimone 1998) that helps the selection of critical features to be learned, and stabilizes synaptic plasticity to prevent catastrophic forgetting.

A vigilance signal, by controlling the matching criterion in target neural networks, can regulate how coarse (general) or fine (concrete) learned categories will become to reflect changing environmental statistics. Vigilance can change due to internal factors, such as fatigue, or external factors, such as surprise or punishment. A baseline vigilance determines how large of a mismatch is initially tolerated before cortical representations are reset and new representation are instated. When a predictive error causes a mismatch to occur, the vigilance level is increased just enough to drive a memory search, or hypothesis testing, for a new recognition code. This process is called *match tracking* (Carpenter and Grossberg 1987). Match tracking realizes a kind of *minimax learning rule*; namely, it enables a learning system to minimize predictive error while maximizing generalization. Choosing a low baseline vigilance leads to the learning of general categories and thus a minimum use of memory resources.

4.3 Sustained vs transient vigilance control and ACh

Vigilance operates over multiple timescales, from the rapid transients during pattern matching processes to the contextual or task-based setting of baseline vigilance levels. Recently developed techniques in the measurement of ACh confirm that concentration transients can occur rapidly at the timescale of a behavioral episode (Parikh et al. 2007; Sarter et al. 2009). Meanwhile, at slower timescales, ACh levels are known to oscillate with circadian rhythms (Crouzier et al. 2006; Marrosu et al. 1995; Williams et al. 1994), increase with caffeine administration through its action as an adenosine receptor antagonist (Carter et al. 1995; Kurokawa et al. 1996), and vary in a task-dependent manner that correlates with attentional demands as confirmed by microdialysis (Arnold et al. 2002; Marrosu et al. 1995) and newer techniques (Parikh et al. 2007).

The largest fluctuations in vigilance may be expected during tasks which require rapid learning of novel information in an ART system. Indeed, activity of the nucleus basalis of Meynert facilitates plasticity of cortical maps both in primary auditory cortex (Kilgard and Merzenich 1998) and in motor cortex (Ramanathan et al. 2009). Specifically, as a result of match tracking, we expect the highest levels of vigilance, and consequently ACh, for incorporating novel exemplars into memory during mismatch processing, and lower levels of ACh for refining of category representations during match episodes. This depiction elucidates recent studies of the effects of scopolamine on human memory formation which suggest that high levels of ACh promote rapid encoding, whereas low levels of ACh support consolidation (Rasch et al. 2006).

Similar studies with scopolamine make the claim that lowering ACh improves consolidation by preventing possible interference with conflicting information (Winters et al. 2007).

4.4 ACh modulation of learned category generality
ART further suggests that baseline vigilance signaling sets the criterion for expectation mismatch and novelty detection. This baseline vigilance level indirectly determines pattern or category specificity. Namely, with low baseline vigilance, an ART system tends to form more general, or abstract, categories over the feature space, while with high baseline vigilance, the system forms more specific, or concrete, categories. Correspondingly, object discrimination studies in rats show that the cholinergic blocker scoplamine reduces the novelty discrimination ratio (Ballaz 2009). ART further suggests behavioral experiments that can distinguish this learning specificity. For example, general category representations may lead to failure to discriminate when a task involves pattern interference; that is, featural overlap across categories. Lesions in rats of the nucleus basalis of Meynert have shown little impact on learning rate, except when there is a high degree of interference between the categories to be learned; that is, when categories share the same features in a certain dimension (Botly and De Rosa, 2007, 2009). Similarly, studies in humans show that scopolamine, by blocking ACh, diminishes learning of overlapping word pairs more than non-overlapping pairs (Atri et al. 2004). Essentially, a lower vigilance causes the system to permit a pattern match with a stimulus of overlapping features, whereas a high vigilance might enable detection of mismatch for the same stimulus. Associative learning studies in rats with combinations of light and tone have shown that the concentration of released ACh increases more during negative patterning discrimination, in which an individual stimulus (A, e.g. light) signals reward and a compound stimulus (AB, e.g. light + tone) signals no reward, than during elemental discrimination, in which one stimulus (A, e.g. light) signals reward and another stimulus (B, e.g. tone) signals no reward (Hata et al. 2007).

How does the cholinergic system manage to regulate learned interference through its diffuse influence over the thalamocortical hierarchy? Our model suggests that this may occur in part via the modulation of the transfer function threshold that, in turn, controls the degree of competition in a target neural population, as demonstrated in rate-based models (Grossberg and Levine 1975). One possible mechanism is the regulation of oscillatory behavior between cortical layers as suggested by Grossberg and Versace (2008). The resultant asynchrony between neurons promotes pattern differentiation, as observed in the primary auditory cortex of the rat (Pandya et al. 2005). Further, this cholinergic modulation may additionally control learning by inducing persistent effects on AHP currents. In concordance with this, attention-demanding learning tasks, in which ACh is expected to play a role, cause long-term changes in both fAHP conductance and sAHP conductance (Matthews et al. 2009; Saar and Barkai 2003).

Architecturally, the cholinergic system operates within a cortical hierarchy, which supports the type of top-down attentional dynamics that are clarified by ART. For instance, activation of cholinergic receptors in prefrontal cortex indirectly increases ACh release in posterior parietal cortex, though the reverse relationship does not occur (Nelson et al. 2005). Further, studies of auditory cortex on mice *in vitro* have demonstrated a synaptic bias in cholinergic modulation, which via muscarinic activation suppresses intracortical synaptic communication, while exerting less suppression of thalamocortical sensory signals (Hsieh et al. 2000). A model of primary auditory cortex by Soto and colleagues explores several possible network effects of cholinergic modulation such as widening or narrowing of excitatory and inhibitory connectivity (Soto et al. 2006).

Finally, the model presented here can be extended to treat cases in which changes in AHP occur independently from ACh modulation. Recent evidence shows that long-term effects on AHP currents, which emerge during rule learning tasks, often continue to manifest themselves after the cholinergic stimulation has subsided (Saar et al. 2001). For example, fear conditioning increases sAHP currents, but does not alter the magnitude of fAHP currents in the prefrontal cortex of rats, leading to a habituation of both output intensity and behavior (Santini et al. 2008). Recent evidence has shown that stimulation with a mixture of different neurotransmitters often produce the additive combination of each individual modulatory effect (Satake et al. 2008). Our model provides a foundation upon which such extensions may be considered.

References

Abel, H. J., Lee, J. C. F., Callaway, J. C., & Foehring, R. C. (2004). Relationships between intracellular calcium and afterhyperpolarizations in neocortical pyramidal neurons. *Journal of Neurophysiology*, 91(1), 324-335.

Akins, P. T., Surmeier, D. J., & Kitai, S. T. (1990). Muscarinic modulation of a transient k+ conductance in rat neostriatal neurons. *Nature*, 344, 240-242.

Anwar, H., Hong, S., & De Schutter, E. (2010). Controlling ca(2+)-activated K (+) channels with models of Ca (2+) buffering in purkinje cells. *Cerebellum* (London, England).

Arnold, H. M., Burk, J. A., Hodgson, E. M., Sarter, M., & Bruno, J. P. (2002). Differential cortical acetylcholine release in rats performing a sustained attention task versus behavioral control tasks that do not explicitly tax attention. *Neuroscience*, 114(2), 451-460.

Atri, A., Sherman, S., Norman, K. A., Kirchhoff, B. A., Nicolas, M. M., Greicius, M. D., Cramer, S. C., Breiter, H. C., Hasselmo, M. E., & Stern, C. E. (2004). Blockade of central cholinergic receptors impairs new learning and increases proactive interference in a word paired-associate memory task. *Behavioral Neuroscience*, 118(1), 223-236.

Ballaz, S. J. (2009). Differential novelty detection in rats selectively bred for novelty-seeking behavior. *Neuroscience Letters*, 461(1), 45-48.

Barkai, E. & Hasselmo, M. E. (1994). Modulation of the input/output function of rat piriform cortex pyramidal cells. *Journal of Neurophysiology*, 72(2), 644-658.

Botly, L. C. & De Rosa, E. (2007). Cholinergic influences on feature binding. *Behavioral neuroscience*, 121(2), 264-276.

Botly, L. C. & De Rosa, E. (2009). Cholinergic deafferentation of the neocortex using 192 igg-saporin impairs feature binding in rats. *Journal of Neuroscience*, 29(13), 4120-4130.

Bordey, A., Sontheimer, H., & Trouslard, J. (2000). Muscarinic activation of BK channels induces membrane oscillations in glioma cells and leads to inhibition of cell migration. *Journal of Membrane Biology*, 176(1), 31-40.

Bosking, W.H., Zhang, Y., Schofield, B., & Fitzpatrick, D. (1997). Orientation selectivity and the arrangement of horizontal connections in the tree shrew striate cortex. *Journal of Neuroscience, 7*, 2112-2127.

Brown, A. M., Schwindt, P. C., & Crill, W. E. (1993). Voltage dependence and activation kinetics of pharmacologically defined components of the high-threshold calcium current in rat neocortical neurons. *Journal of neurophysiology*, 70(4), 1530-43.

Bullier, J., McCourt, M.E., & Henry, G.H. (1988). Physiological studies on the feedback connection to the striate cortex from cortical areas 18 and 19 of the cat. *Experimental Brain Research*, 70, 90–98.

Bullock, D., Cisek, P., & Grossberg, S. (1998). Cortical networks for control of voluntary arm movements under variable force conditions. *Cerebral Cortex*, 8, 48-62.

Bullock, D., & Grossberg, S. (1988). Neural dynamics of planned arm movements: Emergent invariants and speed-accuracy properties during trajectory formation. *Psychological Review*, 95, 49-90.

Canavier, C. C., Oprisan, S. a, Callaway, J. C., Ji, H., & Shepard, P. D. (2007). Computational model predicts a role for ERG current in repolarizing plateau potentials in dopamine neurons: implications for modulation of neuronal activity. *Journal of Neurophysiology*, 98(5), 3006-22.

Cantrell A.R., & Catterall W.A. (2001). Neuromodulation of Na+ channels: an unexpected form of cellular plasticity. *Nature Review Neuroscience*, 2, 397-407.

Carpenter, G.A., & Grossberg, S. (1987) A massively parallel architecture for a self-organizing neural pattern recognition machine, *Computer Vision, Graphics, and Image Processing*, 37, 54-115.

Carpenter, G.A., & Grossberg, S. (1991). *Pattern recognition by self-organizing neural Networks. Cambridge*, MA: MIT Press.

Carter, A. J., O'Connor, W. T., Carter, M. J., & Ungerstedt, U. (1995). Caffeine enhances acetylcholine release in the hippocampus in vivo by a selective interaction with adenosine a1 receptors. *Journal of Pharmacology and Experimental Therapeutics*, 273(2), 637-642.

Chisum, H.J., Mooser, F., & Fitzpatrick, D. (2003). Emergent properties of Layer 2/3 neurons reflect the collinear arrangement of horizontal connections in tree shrew visual cortex. *Journal of Neuroscience, 23*, 2947-2960.

Crouzier, D., Baubichon, D., Bourbon, F., & Testylier, G. (2006). Acetylcholine release, EEG spectral analysis, sleep staging and body temperature studies: A multiparametric approach on freely moving rats. *Journal of Neuroscience Methods*, 151(2), 159-167.

Cox, D. H., Cui, J., & Aldrich, R.W. (1997). Allosteric gating of a large conductance ca-activated K+ channel. *Journal of General Physiology*, 110(3), 257-281.

Delcour, A. H., Lipscombe, D., & Tsien, R. W. (1993). Multiple modes of n-type calcium differences in gating kinetics channel activity distinguished by differences in gating kinetics. *Journal of Neuroscience*, 13(1), 181-194.

Descarries, L. & Umbriaco, D. (1995). Ultrastructural basis of monoamine and acetylcholine function in cns. *Seminars in Neuroscience*, 7(5), 309-318.

Desimone, R. (1998). Visual attention mediated by biased competition in extrastriate visual cortex. *Philosophical Transactions of Royal Socociety B*. 353, 1245–1255.

Destexhe, A., Mainen, Z. F., & Sejnowski, T. J. (1994a). Synthesis of models for excitable membranes, synaptic transmission and neuromodulation using a common kinetic formalism. *Journal of Computational Neuroscience*, 1(3), 195-230.

Destexhe, A., Mainen, Z. F., & Sejnowski, T. J. (1994b). An efficient method for computing synaptic conductances based on a kinetic model of receptor binding. *Neural Computation*, 6(1), 14-18.

Ellias, S., & Grossberg, S. (1975). Pattern formation, contrast control, and oscillations in the short term memory of shunting on-center off-surround networks. *Biological Cybernetics,* 20, 69-98.

Elman, J. L. (1991). Distributed representations, simple recurrent networks, and grammatical structure. *Machine Learning*, 7(2-3), 195-225.

Engel, A.K., Fries, P., & Singer, W., (2001). Dynamic predictions: oscillations and synchrony in top-down processing. *Nature Reviews Neuroscience*, 2, 704–716.

Fellous, J.-M. M., Rudolph, M., Destexhe, A., & Sejnowski, T. J. (2003). Synaptic background noise controls the input/output characteristics of single cells in an in vitro model of in vivo activity. *Neuroscience*, 122(3), 811-829.

Freeman, W. J. (1979). Nonlinear gain mediating cortical stimulus-response relations. *Biological Cybernetics*, 33(4), 237-247.

Fries, P., Reynolds, J.H., Rorie, A.E., & Desimone, R. (2001). Modulation of oscillatory neuronal synchronization by selective visual attention. *Science*, 291, 1560–1563.

Gao, E., & Suga, N. (1998). Experience-dependent corticofugal adjustment of midbrain frequency map in bat auditory system. *Proceedings of the National Academy of Sciences of the United States of America*, 95, 12663–12670.

Giocomo, L., & Hasselmo, M. (2007). Neuromodulation by glutamate and acetylcholine can change circuit dynamics by regulating the relative influence of afferent input and excitatory feedback. *Molecular Neurobiology*, 36(2), 184-200.

Goldman, D. E. (1943). Potential, impedance, and rectification in membranes. *The Journal of General Physiology* 27:37-60.

Grossberg, S. (1973). Contour enhancement, short-term memory, and constancies in reverberating neural networks. *Studies in Applied Mathematics*, 52, 213-257.

Grossberg, S. (1980). How does a brain build a cognitive code? *Psychological Review*, 87, 1–51.

Grossberg, S. (1999). How does the cerebral cortex work? Learning, attention, and grouping by the laminar circuits of visual cortex. *Spatial Vision*, 12, 163–186.

Grossberg, S. (2003). How does the cerebral cortex work? Development, learning, attention, and 3D vision by laminar circuits of visual cortex. *Behavioral and Cognitive Neuroscience Reviews*, 2, 47–76.

Grossberg, S. & Levine, D. (1975). Some developmental and attentional biases in the contrast enhancement and short term memory of recurrent neural networks. *Journal of Theoretical Biology*, 53(2), 341-380.

Grossberg, S. & Versace, M. (2008). Spikes, synchrony, and attentive learning by laminar thalamocortical circuits. *Brain Research*, 1218, 278-312.

Hata, T., Kumai, K., & Okaichi, H. (2007). Hippocampal acetylcholine efflux increases during negative patterning and elemental discrimination in rats. *Neuroscience Letters*, 418(2), 127-132.

Hestrin, S. & Armstrong, W. E. (1996). Morphology and physiology of cortical neurons in layer i. *Journal of Neuroscience*, 16(17), 5290-5300.

Hicks, G. A. & Marrion, N. V. (1998). Ca2+-dependent inactivation of large conductance Ca2+-activated K+ (BK) channels in rat hippocampal neurones produced by pore block from an associated particle. *Journal of Physiology*, 508 (3), 721-734.

Hirschberg, B., Maylie, J., Adelman, J. P., & Marrion, N. V. (1998). Gating of recombinant small-conductance Ca-activated K+ channels by calcium. *Journal of General Physiology*, 111(4), 565-81.

Hodgkin, A. L. & Huxley, A. F. (1952). Currents carried by sodium and potassium ions through the membrane of the giant axon of loligo. *Journal of Physiology*, 116(4), 449-472.

Hodgkin, A. L. & Katz, B. (1949). The effect of sodium ions on the electrical activity of the giant axon of the squid. *The Journal of Physiology* 108:37-77.

Hotson, J. R. & Prince, D. A. (1980). A calcium-activated hyperpolarization follows repetitive firing in hippocampal neurons. *Journal of Neurophysiology*, 43(2), 409-419.

Hsieh, C. Y., Cruikshank, S. J., & Metherate, R. (2000). Differential modulation of auditory thalamocortical and intracortical synaptic transmission by cholinergic agonist. *Brain Research*, 880(1-2), 51-64.

Karmarkar, U. R., & Buonomano, D. V. (2006). Different forms of homeostatic plasticity are engaged with distinct temporal profiles. *The European journal of neuroscience*, *23*(6), 1575-84.

Kilgard, M. P. & Merzenich, M. M. (1998). Cortical map reorganization enabled by nucleus basalis activity. *Science*, 279(5357), 1714-1718.

King, J. D., & Meriney, S. D. (2005). Proportion of N-type calcium current activated by action potential stimuli. *Journal of Neurophysiology*, 94(6), 3762-70.

Klink, R. & Alonso, A. (1997). Muscarinic modulation of the oscillatory and repetitive firing properties of entorhinal cortex layer II neurons. *Journal of Neurophysiology*, 77(4), 1813-1828.

Köhn, J. & Wörgötter, F. (1998). Employing the zeta-transform to optimize the calculation of the synaptic conductance of NMDA and other synaptic channels in network simulations. *Neural Computation*, 10(7), 1639-1651.

Kong, W.-J. J., Guo, C.-K. K., Zhang, S., Hao, J., Wang, Y.-J. J., & Li, Z.-W. W. (2005). The properties of ach-induced BK currents in guinea pig type ii vestibular hair cells. *Hearing Research*, 209(1-2), 1-9.

Kong, W.-J. J., Guo, C.-K. K., Zhang, X.-W. W., Chen, X., Zhang, S., Li, G.-Q. Q., Li, Z.-W. W., & Van Cauwenberge, P. (2007). The coupling of acetylcholine-induced BK channel and calcium channel in guinea pig saccular type ii vestibular hair cells. *Brain Research*, 1129(1), 110-115.

Köppen, A., Klein, J., Schmidt, B. H., van der Staay, F. J., & Löffelholz, K. (1996). Effects of nicotinamide on central cholinergic transmission and on spatial learning in rats. *Pharmacology, Biochemistry, and Behavior*, 53(4), 783-790.

Kraus, N., McGee, T., Littman, T., Nicol, T., & King, C. (1994). Nonprimary auditory thalamic representation of acoustic change. *Jounral of Neurophysiology*, 72, 1270–1277.

Krause, M. & Pedarzani, P. (2000). A protein phosphatase is involved in the cholinergic suppression of the Ca(2+)-activated K(+) current sI(AHP) in hippocampal pyramidal neurons. *Neuropharmacology*, 39(7), 1274-1283.

Krupa, D.J., Ghazanfar, A.A., & Nicolelis, M.A.L. (1999). Immediate thalamic sensory plasticity depends on corticothalamic feedback. *Proceedings of the National Academy of Sciences of the United States of America*, 96, 8200–8205.

Kurokawa, M., Shiozaki, S., Nonaka, H., Kase, H., Nakamura, J., & Kuwana, Y. (1996). In vivo regulation of acetylcholine release via adenosine a1 receptor in rat cerebral cortex. *Neuroscience Letters*, 209(3), 181-184.

Lancaster, B. & Adams, P. R. (1986). Calcium-dependent current generating the afterhyperpolarization of hippocampal neurons. *Journal of Neurophysiology*, 55(6), 1268-1282.

Lee, J. C. F., Callaway, J. C., & Foehring, R. C. (2005). Effects of temperature on calcium transients and ca2+-dependent afterhyperpolarizations in neocortical pyramidal neurons. *Journal of Neurophysiology*, 93(4), 2012-2020.

Levitt, J.B., Yoshioka, T., & Lund, J.S. (1994). Intrinsic cortical connections in macaque visual area V2: evidence for interaction between different functional streams. *Journal of Comparative Neurology, 342*, 551-570.

Lima, P. A. & Marrion, N. V. (2007). Mechanisms underlying activation of the slow ahp in rat hippocampal neurons. *Brain Research*, 1150, 74-82.

Loane, D. J., Lima, P. a, & Marrion, N. V. (2007). Co-assembly of N-type Ca2+ and BK channels underlies functional coupling in rat brain. *Journal of Cell Science*, 120(Pt 6), 985-95.

Lorenzon, NM, & Foehring, RC. (1992). Relationship Between Repetitive Firing and Afterhyperpolarizations in Human Neocortical Neurons. *Journal of Neurophysiology*, 67(2), 350-363.

Lorenzon, N. M., & Foehring, R. C. (1995). Characterization of pharmacologically identified voltage-gated calcium channel currents in acutely isolated rat neocortical neurons. *Journal of neurophysiology*, 73(4), 1430-42.

Luvisetto, S., Fellin, T., Spagnolo, M., Hivert, B., Brust, P. F., Harpold, M. M., Stauderman, K. A., Williams, M. E., & Pietrobon, D. (2004). Modal gating of human CaV2.1 (P/Q-type) calcium channels: I. the slow and the fast gating modes and their modulation by beta subunits. *Journal of General Physiology*, 124(5), 445-61.

Marrosu, F., Portas, C., Mascia, M., Casu, M., Fa, M., Giagheddu, M., Imperato, A., & Gessa, G. (1995). Microdialysis measurement of cortical and hippocampal acetylcholine release during sleep-wake cycle in freely moving cats. *Brain Research*, 671(2), 329-332.

Markram, H., Lübke, J., Frotscher, M., & Sakmann, B. (1997). Regulation of synaptic efficacy by coincidence of postsynaptic aps and epsps. *Science*, 275(5297), 213-215.

Matthews, E. A., Linardakis, J. M., & Disterhoft, J. F. (2009). The fast and slow afterhyperpolarizations are differentially modulated in hippocampal neurons by aging and learning. *Journal of Neuroscience*, 29(15), 4750-4755.

McCormick, D. A. & Williamson, A. (1989). Convergence and divergence of neurotransmitter action in human cerebral cortex. *Proceedings of the National Academy of Sciences of the United States of America*, 86(20), 8098-8102.

Mechawar, N., Watkins, K. C., & Descarries, L. (2002). Ultrastructural features of the acetylcholine innervation in the developing parietal cortex of rat. *Journal of Comparative Neurology*, 443(3), 250-258.

Mitchell, J., Sundberg, K., & Reynolds, J. (2007). Differential attention-dependent response modulation across cell classes in macaque visual area v4. *Neuron*, 55(1), 131-141.

Morishima, M., & Kawaguchi, Y. (2006). Recurrent connection patterns of corticostriatal pyramidal cells in frontal cortex. *The Journal of Neuroscience*, *26*(16), 4394-4405.

Muller, W., Petrozzino, J. J., Griffith, L. C., Danho, W., & Connor, J. A. (1992). Specific involvement of ca(2+)-calmodulin kinase II in cholinergic modulation of neuronal responsiveness. *Journal of Neurophysiology*, 68(6), 2264-2269.

Nakajima, Y., Nakajima, S., Leonard, R. J., & Yamaguchi, K. (1986). Acetylcholine raises excitability by inhibiting the fast transient potassium current in cultured hippocampal neurons. *Proceedings of the National Academy of Sciences of the United States of America*, 83(9), 3022-3026.

Nelson, C. L., Sarter, M., & Bruno, J. P. (2005). Prefrontal cortical modulation of acetylcholine release in posterior parietal cortex. *Neuroscience*, 132(2), 347-359.

Pandya, P. K., Moucha, R., Engineer, N. D., Rathbun, D. L., Vazquez, J., & Kilgard, M. P. (2005). Asynchronous inputs alter excitability, spike timing, and topography in primary auditory cortex. *Hearing Research*, 203(1-2), 10-20.

Parikh, V., Kozak, R., Martinez, V., & Sarter, M. (2007). Prefrontal acetylcholine release controls cue detection on multiple timescales. *Neuron*, 56(1), 141-154.

Parikh, V. & Sarter, M. (2006). Cortical choline transporter function measured in vivo using choline-sensitive microelectrodes: clearance of endogenous and exogenous choline and effects of removal of cholinergic terminals. *Journal of Neurochemistry*, 97(2), 488-503.

Pedarzani, P. & Storm, J. F. (1996). Evidence that ca/calmodulin-dependent protein kinase mediates the modulation of the Ca2+-dependent K+ current, Iahp, by acetylcholine, but not by glutamate, in hippocampal neurons. *Pflügers Archival European Journal of Physiology*, 431(5), 723-728.

Pineda, J. C., Waters, R. S., & Foehring, R. C. (1998). Specificity in the interaction of HVA Ca2+ channel types with Ca2+-dependent AHPs and firing behavior in neocortical pyramidal neurons. *Journal of Neurophysiology*, 79(5), 2522-34.

Pollen, D.A. (1999). On the neural correlates of visual perception. *Cerebral Cortex*, 9, 4–19.

Power, J. M. & Sah, P. (2008). Competition between calcium-activated k+ channels determines cholinergic action on firing properties of basolateral amygdala projection neurons. *Journal of Neuroscience*, 28(12), 3209-3220.

Povysheva, N. V., Gonzalez-Burgos, G., Zaitsev, A. V., Kroner, S., Barrionuevo, G., Lewis, D. A., & Krimer, L. S. (2006). Properties of excitatory synaptic responses in fast-spiking interneurons and pyramidal cells from monkey and rat prefrontal cortex. *Cerebral Cortex*, 16(4), 541-552.

Prakriya, M. & Lingle, C. J. (1999). BK channel activation by brief depolarizations requires Ca2+ influx through L- and Q-type Ca2+ channels in rat chromaffin cells. *Journal of Neurophysiology*, 81(5), 2267-2278.

Prakriya, M., Solaro, C. R., & Lingle, C. J. (1996). [Ca2+]i elevations detected by BK channels during Ca2+ influx and muscarine-mediated release of Ca2+ from intracellular stores in rat chromaffin cells. *Journal of Neuroscience*, 16(14), 4344-4359.

Prinz, AA, Billimoria, CP, & Marder, E. (2003). Alternative to Hand-Tuning Conductance-Based Models: Construction and Analysis of Databases of Model Neurons. *Journal of Neurophysiology,* 90, 3998-4015.

Ramanathan, D., Tuszynski, M. H., & Conner, J. M. (2009). The basal forebrain cholinergic system is required specifically for behaviorally mediated cortical map plasticity. *Journal of Neuroscience*, 29(18), 5992-6000.

Rasch, B. H., Born, J., & Gais, S. (2006). Combined blockade of cholinergic receptors shifts the brain from stimulus encoding to memory consolidation. *Journal of cognitive neuroscience*, 18(5), 793-802.

Rhodes, P.A., & Gray, C. M. (1994). Simulations of intrinsically bursting neocortical pyramidal neurons. *Neural Computation*, 6(6), 1086-1110.

Saar, D., Grossman, Y., & Barkai, E. (2001). Long-lasting cholinergic modulation underlies rule learning in rats. *Journal of Neuroscience*, 21, 1385–1392.

Saar, D. & Barkai, E. (2003). Long-term modifications in intrinsic neuronal properties and rule learning in rats. *European Journal of Neuroscience*, 17, 2727–2734.

Sah, P. (1996). Ca(2+)-activated K+ currents in neurones: types, physiological roles and modulation. *Trends in Neuroscience*, 19(4), 150-154.

Santini, E., Quirk, G. J., & Porter, J. T. (2008). Fear conditioning and extinction differentially modify the intrinsic excitability of infralimbic neurons. *Journal of Neuroscience*, 28(15), 4028-4036.

Sarter, M, Hasselmo, ME, Bruno, JP, & Givens, B. (2005). Unraveling the Attentional Functions of Cortical Cholinergic Inputs: Interactions between signal-driven and cognitive modulation of signal detection. *Brain Research Reviews*, 48, 98-111.

Sarter, M., Parikh, V., & Howe, W.M. (2009). Phasic acetylcholine release and the volume transmission hypothesis: time to move on. *Nature Reviews Neuroscience*, 10(5), 383-390.

Satake, T., Mitani, H., Nakagome, K., & Kaneko, K. (2008). Individual and additive effects of neuromodulators on the slow components of afterhyperpolarization currents in layer v pyramidal cells of the rat medial prefrontal cortex. *Brain Research*, 1229, 47-60.

Schmidt, K.E., Goebel, R. Löwel, S., & Singer, W. (1997). The perceptual grouping criterion of colinearity is reflected by anisotropies of connections in the primary visual cortex. *European Journal of Neuroscience, 9*, 1083-1089.

Schreiber, M. & Salkoff, L. (1997). A novel calcium-sensing domain in the BK channel. *Biophysical Journal*, 73(3), 1355-1363.

Schwindt, P.C., Spain, W.J., Foehring, R.C., Stafstrom, C.E., Chubb, M.C., & Crill, W.E. (1988a). Multiple potassium conductances and their functions in neurons from cat sensorimotor cortex in vitro. *Journal of Neurophysiology*, 59, 424-449.

Schwindt, P.C., Spain, W.J., Foehring, R.C., Stafstrom, C.E., Chubb, M.C., & Crill, W.E. (1988b). Slow conductances in neurons from cat sensorimotor cortex in vitro and their role in excitability changes. *Journal of Neurophysiology*, 59, 450-467.

Shapiro, M.S., Roche, J.P., Kaftan, E.J., Cruzblanca, H., Mackie, K., & Hille, B. (2000). Reconstitution of muscarinic modulation of the KCNQ2/KCNQ3 K(+) channels that underlie the neuronal M current. *Journal of Neuroscience*, 20(5), 1710-1721.

Sillito, A.M., Jones, H.E., Gerstein, G.L., & West, D.C. (1994). Feature-linked synchronization of thalamic relay cell firing induced by feedback from the visual cortex. *Nature*, 369, 479–482.

Solinas, S., Forti, L., Cesana, E., Mapelli, J., De Schutter, E., & D'Angelo, E. (2007). Computational reconstruction of pacemaking and intrinsic electroresponsiveness in cerebellar golgi cells. *Frontiers in Cellular Neuroscience*, 1(12), 2.

Song, S., Sjöström, P.J., Reigl, M., Nelson, S., & Chklovskii, D.B. (2005). Highly nonrandom features of synaptic connectivity in local cortical circuits. *PLoS Biology,* 3(3): 507-519.

Soto, G, Kopell, N, & Sen, K. (2006). Network Architecture, Receptive Fields, and Neuromodulation: Computational and Functional Implications of Cholinergic Modulation in Primary Auditory Cortex. *Journal of Neurophysiology*, 96: 2972-2983.

Storm, J. F. (1987). Action potential repolarization and a fast after-hyperpolarization in rat hippocampal pyramidal cells. *Journal of Physiology*, 385(1), 733-759.

Storm, J. F. (1989). An after-hyperpolarization of medium duration in rat hippocampal pyramidal cells. *Journal of Physiology*, 409, 171-190.

Sun, X., Gu, X. Q., & Haddad, G. G. (2003). Calcium influx via L- and N-type calcium channels activates a transient large-conductance Ca2+-activated K+ current in mouse neocortical pyramidal neurons. The Journal of Neuroscience, 23(9), 3639-48.

Taylor, AL, Hickey, TJ, Prinz, AA, & Marder, E. (2006). Structure and visualization of high-dimensional conductance spaces. *Journal of Neurophysiology*, 96, 891-905.

Traub, R.D., Buhl, E. H., Gloveli, T., & Whittington, M.A. (2003). Fast rhythmic bursting can be induced in layer 2/3 cortical neurons by enhancing persistent Na+ conductance or by blocking BK channels. Journal of Neurophysiology, 89(2), 909-21.

Traub, R. D., Contreras, D., Cunningham, M. O., Murray, H., LeBeau, F. E., Roopun, A., Bibbig, A., Wilent, W. B., Higley, M. J., & Whittington, M. A. (2005). Single-column thalamocortical network model exhibiting gamma oscillations, sleep spindles, and epileptogenic bursts. *Journal of Neurophysiology,* 93, 2194-2232.

Traub, R.D., Wong, RK, Miles, R, & Michelson, H. (1991). A model of a CA3 hippocampal pyramidal neuron incorporating voltage-clamp data on intrinsic conductances. *Journal of Neurophysiology*, 66(2), 635-650.

Turrigiano, G., Abbott, L. F., & Marder, E. (1994). Activity-dependent changes in the intrinsic properties of cultured neurons. Science 264:974-977.

Umbriaco, D., Watkins, K.C., Descarries, L., Cozzari, C., & Hartman, B.K. (1994). Ultrastructural and morphometric features of the acetylcholine innervation in adult rat parietal cortex: an electron microscopic study in serial sections. *Journal of Comparative Neurology*, 348(3), 351-373.

Usrey, W.M. (2002). The role of spike timing for thalamocortical processing. *Current Opinion in Neurobiology*, 12, 411–417.

van Der Werf, Y.D., Witter, M.P., & Groenewegen, H.J. (2002). The intralaminar and midline nuclei of the thalamus. Anatomical and functional evidence for participation in processes of arousal and awareness. *Brain Research Reviews*, 39, 107–140.

Van Geit, W., Achard, P., & De Schutter, E. (2007). Neurofitter: A parameter tuning package for a wide range of electrophysiological neuron models. *Frontiers in Neuroinformatics*, 1, 1-17.

Versace, M., Ames, H., Léveillé, J., Fortenberry, B., & Gorchetchnikov, A. (2008). Kinness: a modular framework for computational neuroscience. *Neuroinformatics*, 6, 291-309.

Villalobos, C., Shakkottai, V.G., Chandy, K.G., Michelhaugh, S.K., & Andrade, R. (2004). SK_{ca} channels mediate the medium but not the slow calcium-activated afterhyperpolarization in cortical neurons. *Journal of Neuroscience*, 24(14), 3537-3542.

Vogalis, F., Storm, J.F., & Lancaster, B. (2003). SK channels and the varieties of slow after-hyperpolarizations in neurons. *European Journal of Neuroscience*, 18, 3155-3166.

Wallner, M., Meera, P., & Toro, L. (1999). Molecular basis of fast inactivation in voltage and Ca2+-activated K+ channels: a transmembrane beta-subunit homolog. *Proceedings of the National Academy of Sciences of the United States of America*, 96(7), 4137-4142.

Watt, A., van Rossum, M., MacLeod, K., Nelson, S., & Turrigiano, G. (2000). Activity coregulates quantal AMPA and NMDA currents at neocortical synapses. *Neuron*, 26(3), 659-670.

Wang, X.J., Liu,Y., Sanchez-Vives, M.V., & McCormick, D.A. (2003). Adaptation and temporal decorrelation by single neurons in the primary visual cortex. *Journal of Neurophysiology*, 89, 3279-3293.

Weaver, C.M., & Wearne, S.L. (2008). Neuronal Firing Sensitivity to Morphologic and Active Mebrane Parameters. *PLoS Computational Biology*, 4(1), 130-150.

Wei, A. D., Gutman, G. A., Aldrich, R., Chandy, K. G., Grissmer, S., & Wulff, H. (2005). International union of pharmacology. LII. nomenclature and molecular relationships of calcium-activated potassium channels. *Pharmacological Reviews*, 57(4), 463-472.

Wersing, H., Beyn, W., & Ritter, H. (2001). Dynamical stability conditions for recurrent neural networks with unsaturating piecewise linear transfer functions. *Neural Computation*, 13, 1811-1825.

Williams, J.A., Comisarow, J., Day, J., Fibiger, H.C., & Reiner, P.B. (1994). State-dependent release of acetylcholine in rat thalamus measured by in vivo microdialysis. *Journal of Neuroscieince*, 14(9), 5236-5242.

Wilson, C.J., Weyrick, A., Terman, D., Hallworth, N. E., & Bevan, M. D. (2004). A model of reverse spike frequency adaptation and repetitive firing of subthalamic nucleus neurons. Journal of Neurophysiology, 91(5), 1963-80.

Winters, B.D., Bartko, S.J., Saksida, L.M., & Bussey, T.J. (2007). Scopolamine infused into perirhinal cortex improves object recognition memory by blocking the acquisition of interfering object information. *Learning & Memory*, 14(9), 590-596.

Zhang, Y.-q. Q., Lü, S.-g. G., Ji, Y.-p. P., Zhao, Z.-q. Q., & Mei, J. (2004). Electrophysiological and pharmacological properties of nucleus basalis magnocellularis neurons in rats. *Acta Pharmacologica Sinica*, 25(2), 161-170.